Biogeochemical Conditions in the Equatorial Pacific in Late 1994

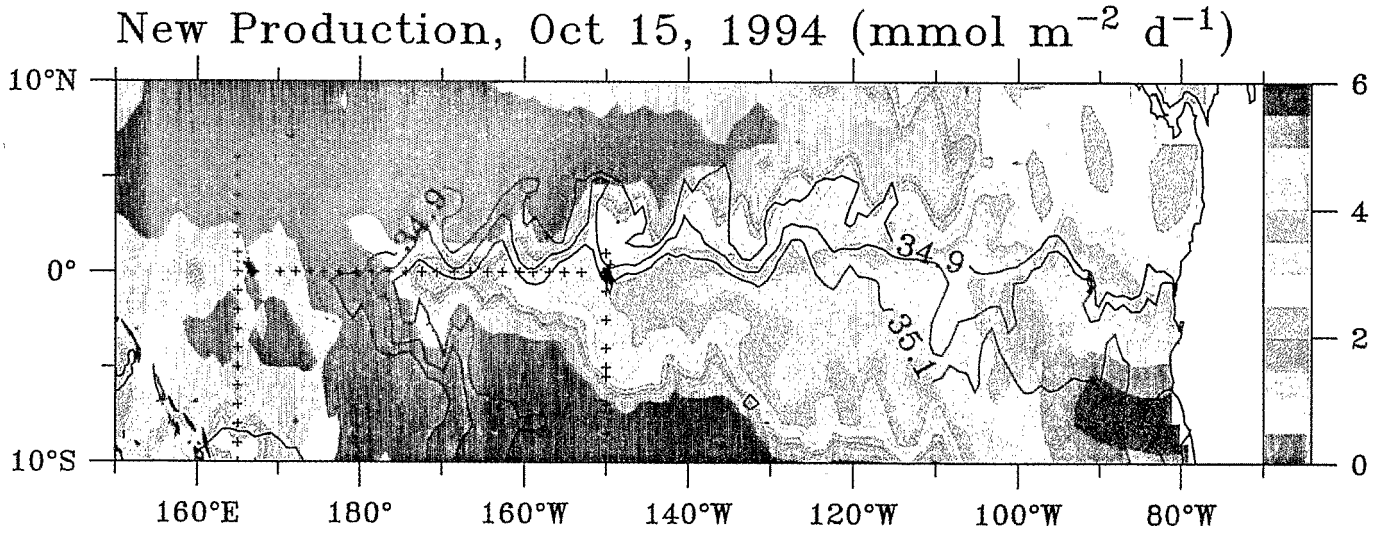

Reprinted from the Journal of Geophysical Research
Published by the American Geophysical Union

JOURNAL OF GEOPHYSICAL RESEARCH, VOL. 104, NO. C2, PAGES 3323–3339, FEBRUARY 15, 1999

The coupled physical-new production system in the equatorial Pacific during the 1992-1995 El Niño

Anne Stoens,[1] Christophe Menkès,[1] Marie-Hélène Radenac,[1] Yves Dandonneau,[1] Nicolas Grima,[1] Gérard Eldin,[2,3] Laurent Mémery,[1] Claudie Navarette,[2] Jean-Michel André,[2] Thierry Moutin,[4] and Patrick Raimbault[4]

Abstract. We investigate the coupling between the physics and new production variability during the period April 1992 to June 1995 in the equatorial Pacific via two cruises and simulations. The simulations are provided by a high-resolution Ocean General Circulation Model forced with satellite-derived weekly winds and coupled to a nitrate transport model in which biology acts as a nitrate sink. The cruises took place in September-October 1994 and sampled the western Pacific warm pool and the upwelling region further east. The coupled model reproduces these contrasted regimes. In the oligotrophic warm pool the upper layer is fresh, and nitrate-depleted, and the new production is low. In contrast, the upwelling waters are colder, and saltier with higher nitrate concentrations, and the new production is higher. Along the equator the eastern edge of the warm pool marked by a sharp salinity front, also coincides with a "new production front". Consistent with the persistent eastward surface currents during the second half of 1994, these fronts undergo huge eastward displacement at the time of the cruises. The warm/fresh pool and oligotrophic region has an average new production of 0.9 mmol NO_3 m^{-2} d^{-1}, which is almost balanced by horizontal advection from the central Pacific and by vertical advection of richer water from the nitrate reservoir below. In contrast, the upwelling mesotrophic region shows average new production of 2.1 mmol NO_3 m^{-2} d^{-1} and the strong vertical nitrate input by the equatorial upwelling is balanced by the losses, through westward advection and meridional divergence of nitrate rich waters, and by the biological sink.

1. Introduction

The major focus of the Joint Global Ocean Flux Study (JGOFS) international program is devoted to the oceanic carbon cycle and its long-term consequences on the variations of the atmospheric CO_2 content. Among JGOFS process studies, those concerning the equatorial Pacific were undertaken for several reasons.

First of all, the equatorial cold tongue of upwelled waters has large spatial extension [*Wyrtki*, 1981]. These waters upwelled from depth are rich in nutrients and in inorganic carbon. High nutrient content enhances photosynthesis, new production of organic carbon, and sedimentation of particles. In addition, the high carbon content of the upwelled waters maintains a high partial pressure of CO_2 at the sea surface. In relation to this, in this region the CO_2 flux at the air-sea interface goes to the atmosphere, and the Pacific equatorial upwelling is the largest marine source of CO_2 to the atmosphere [*Tans et al.*, 1990]. This makes the equatorial Pacific a key region for the carbon cycle.

A second characteristic of the equatorial Pacific is its relatively modest chlorophyll content and low primary productivity compared to the abundance of nitrate in the surface layers. The equatorial Pacific upwelled waters have thus been described as high nutrients-low chlorophyll waters (HNLC) [*Thomas*, 1979] and the roles of iron [*Martin*, 1990; *Barber*, 1992] or of grazing [*Walsh*, 1976] have been proposed to explain this paradox. However, neither the high carbon fluxes to the atmosphere and to depth, which are common to all tropical upwelling areas, nor the HNLC character, which is also observed in the Antarctic, are exclusive of the equatorial Pacific.

In contrast, a third property is unique to this region: it arises from the interannual El Niño-Southern Oscillation (ENSO) that affects the world climate. During the warm phases of this oscillation (El Niño) the equatorial upwelling collapses dramatically reducing the biological sink of carbon associated with new production [*Barber and Chavez*, 1983; *Dandonneau*, 1986] and the CO_2 outgasing [*Wong et al.*, 1984, 1993; *Feely et al.*, 1995; *Dandonneau*, 1995]. The study and prediction of ENSO constituted the major goals of the 1985-1994 international Tropical Ocean Global Atmosphere program (TOGA). In the course of TOGA our general knowledge of large-scale circulation has been greatly improved. It is now well known that the variability of the equatorial Pacific results from basin-wide coupling processes between the ocean and the atmosphere. The circulation of surface water masses, which controls the equatorial upwelling, is deeply affected by these processes. This emphasizes the point that the value of biogeochemical variables at a given position, which results largely from the

[1] Laboratoire d'Océanographie Dynamique et de Climatologie, (CNRS/ORSTOM/Univ. Paris 6), Paris, France.
[2] Institut Français de Recherche Scientifique pour le Développement en Coopération, Nouméa, New Caledonia, France.
[3] Now at Laboratoire d'Etudes en Géophysique et Océanographie Spatiales, Toulouse, France.
[4] Centre d'Océanologie de Marseille, Marseille, France.

Paper number 98JC02713.
0148-0227/99/98JC-02713$09.00

advection of upwelled water, is controlled by these processes and thus cannot be properly understood in a one-dimensional (1-D) view. In particular, horizontal advection is of primary importance for determining the biogeochemical conditions in the equatorial Pacific. This complicates the study of the biological fluxes to such a point that certainly, the JGOFS study of the equatorial Pacific would not have been possible without the lessons from TOGA.

During this program, in situ observational networks such as Tropical Atmosphere Ocean (TAO) have been deployed all over the equatorial Pacific, which deliver, in particular, real-time knowledge of the subsurface thermal structure variations of the ocean (10°S-10°N) and knowledge of the current along the equator [*Hayes et al.*, 1991, *McPhaden*, 1993] so that the equatorial Pacific Ocean is now the best observed ocean. Therefore the international JGOFS study of the equatorial Pacific has benefited from the attainments of TAO. For example, *Kessler and McPhaden* [1995] used these networks to describe of the dynamical aspects of the equatorial Pacific during the period of the U.S.-JGOFS EqPac cruises which sampled the central Pacific Ocean, at 140°W, during a warm anomaly, and during near-normal conditions in spring and fall of 1992 respectively.

The western equatorial Pacific has been studied during an Australian-JGOFS cruise in October 1990 [*Mackey et al.*, 1995] during non El-Niño conditions. The FLUPAC and OLIPAC JGOFS-France cruises in the western to central equatorial Pacific were made in September-November 1994 when conditions were more characteristic of warm conditions. The latter cruises sampled the ocean in dynamically and biogeochemically contrasted areas. In short, the western equatorial Pacific is characterized by a warm pool region where surface waters are warmer and fresher than upwelled waters farther east. This warm pool experiences huge zonal excursions on interannual timescales which are of fundamental importance for the world climate [*Picaut et al.*, 1996]. The signature of these two contrasted physical regimes is also reflected in biogeochemistry as seen in Figure 1 where abundance of 0-500 m integrated mesozooplankton (>200 μm) [*Le Borgne and Rodier*, 1997] as well as other parameters along the equator during FLUPAC increase sharply from the warm pool region to the upwelling region. This suggests a strong coupling between the physics and biogeochemistry at the time of the FLUPAC and OLIPAC cruises.

The main objective of this work is thus to gain knowledge on the coupled dynamical-biogeochemical processes that are at work in the settling, in the maintenance, and in the large-scale displacement of the nutrient poor warm pool and the adjacent waters in relation to ENSO conditions. Thus we aim at understanding the main coupled factors that control new production in the equatorially contrasted waters.

Such knowledge can be gained through observations: for instance, the FLUPAC and OLIPAC cruises were focused on the estimation of new and exported primary production, in relation to the dynamics of the ocean. However, as useful as it may be, such information provided by the FLUPAC and OLIPAC data is only relevant to the place and time where these cruises took place. In order to understand the observations in the large-scale context, it is necessary to enlarge the scope of the punctual cruises to the basin and to the seasonal to interannual scales. While synoptic view of the ocean sea level variations is successfully given by altimeters such as TOPEX/POSEIDON [*Busalacchi et al.*, 1994; *Picaut et al.*, 1995] and dynamic height is monitored by the TAO network, previous attempts to develop such a comprehensive data set for biogeochemical data are limited to satellite-detected sea color by the Coastal Zone Color Scanner [*Yoder et al.*, 1993] and monitoring using measurements by ships of opportunity [*Dandonneau*, 1992]. Therefore the basin-scale link between the physics and the biology can only be inferred from coupled models.

In the equatorial ocean where advection processes, especially by zonal currents, are known to be important [*Picaut and Delcroix*, 1995], 1-D coupled models can generally not account for observed variations, and one needs to use a 3-D coupled model to describe the complexity of observed variability. Coupled biological-physical models in the equatorial Pacific have already been used to study the seasonal variations of the basin and long-term evolution [*Toggweiler and Carson*, 1995; *Chai et al.*, 1996]. Toggweiler and Carson, and Chai et al. used climatological forcing in their simulations which is not appropriate for a case study focused on the situation encountered at the time of FLUPAC and OLIPAC or for understanding the coupled conditions during ENSO period. Similarly, it is not well suited for the study of transient processes such as equatorial and instability waves which propagate in the equatorial region and may deeply impact the biology [*Murray et al.*, 1994].

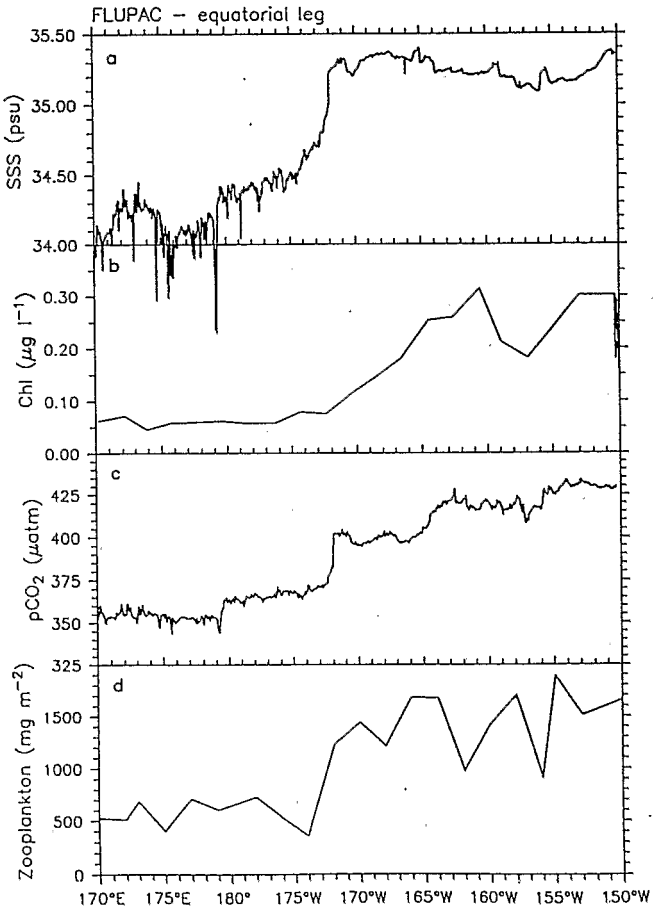

Figure 1. Surface biogeochemical measurements along the equatorial FLUPAC leg: (a) sea surface salinity, (b) chlorophyll, (c) pCO_2 in the ocean, and (d) ash free dry weight of mesozooplankton in the upper 500 m adapted from *Le Borgne and Rodier*, [1997].

In order to explicitly resolve all these features we use here the high-resolution Ocean General Circulation Model (OGCM) OPA of the Laboratoire d'Océanographie Dynamique et de Climatologie (LODYC) [*Blanke and Delecluse*, 1993] forced by high-resolution, high-quality remotely sensed European Remote Sensing (ERS)-1 scatterometer stresses [*Grima et al.*, 1998] and coupled to a nitrate transport model. By this we aim at simulating the physical-new production interactions during the 1992-1994 weak El Niño period in which FLUPAC and OLIPAC took place.

The paper is thus organized as follows: in section 2, data and model descriptions are given. In section 3 a quick overview of the large-scale variations of the physical conditions from 1992 to 1995 is given from data and model fields. The coupled dynamical-biogeochemical modeled situations during the FLUPAC and OLIPAC cruises are then compared to data. In section 4 the variations of coupled dynamical-new production features over the equatorial Pacific from 1992 to 1995 are studied using the model. It is shown that new production at the equator experiences a sharp transition when going from the warm/fresh pool region to the upwelling region and that this transition has large east-west displacements over the basin in association with the ENSO-related east-west displacements of the salinity front at the eastern edge of the warm pool. Finally, discussion about the modeled new production is given, and in section 5 the conclusion is presented.

2. Data and Model

2.1. Materials and Methods Used During FLUPAC and OLIPAC Cruises

The FLUPAC cruise sampled the equatorial Pacific in these two different regimes with a meridional transect along 165°E (20°S-6°N; September 1994), across the oligotrophic waters of the warm pool, and an equatorial section across the eastern edge of the warm pool into the upwelling region (167°E-150°W; October 1994). The OLIPAC meridional transect took place along 150°W (13°S-1°N; November 1994).

Temperature and salinity were obtained using a Sea-Bird SBE 911+ Conductivity-Temperature-Depth profiler (CTD). The sensors were calibrated before the beginning of FLUPAC, and salinity data were validated after measurements of discrete samples with a Portasal salinometer. The vertical profiles of temperature and salinity were processed for spike removal and binned every meter using the software provided by Sea-Bird.

Currents were continuously recorded by two acoustic Doppler current profilers (ADCPs) from R. D. Instruments. The two ADCPs used 75 and 300 kHz frequencies, with vertical resolutions of 16 and 4 m and first bins at 28 and 12 m, respectively. The results from the two instruments were in good agreement, so that the two files of data could be merged into a single set of vertical profiles from 12 to 700 m depth.

Nitrate was measured with a Technicon autoanalyzer using the colorimetric method described by *Strickland and Parsons* [1972]. For low nitrate concentrations this method was improved to detect nitrate at concentrations as low as 0.003 μmole kg^{-1} at FLUPAC [*Oudot and Montel*, 1988] and 0.001 μmole kg^{-1} at OLIPAC [*Raimbault et al.*, 1990].

The chlorophyll concentration was measured according to several techniques (including high-performance liquid chromatography and spectrofluorometry). The data presented here, in order to provide an indication of the biological activity, were obtained using the fluorescence/acidification technique described by *Yentsch and Menzel* [1963], where the pigments are extracted by methanol instead of acetone [*Herbland et al.*, 1985]. Filtration was made on Whatman GF/F filters, filtration pressure being kept below 0.15 atm.

2.2. Data From Observations Networks

Among diverse observing systems enhanced or developed during TOGA the TAO array of deep ocean moorings provides a permanent and synoptic view of the upper ocean thermal structure with high temporal resolution. Dynamic heights deduced from the TAO data were kindly provided by M. McPhaden and D. McClurg at Pacific Marine Environmental Laboratory (PMEL), National Oceanic and Atmospheric Administration (NOAA). These dynamic heights at mooring positions are interpolated onto a regular 5° longitude × 1° latitude × 1 day grid using objective analysis used in *Menkes et al.* [1995]. Together with these in situ data, the *Reynolds and Smith* [1994] sea surface temperatures (SSTs) are used.

2.3. The Dynamical Model

The dynamical model we are using is the three tropical oceans version of the OPA-LODYC OGCM [*Maes et al.*, 1997]. One specificity of this model is the parameterization of vertical diffusion using the 1.5 turbulent kinetic energy (TKE) closure [*Blanke and Delecluse*, 1993]. This high-resolution (45' longitude × 20' latitude at the equator; 16 vertical levels in the upper 150 m) model is forced with observed weekly stresses deduced from ERS-1 scatterometer [*Grima et al.*, 1998]. There is a good agreement between wind vectors from the ERS-1 scatterometer and winds measured on the TAO buoys [*Bentamy et al.*, 1996; *Grima et al.*, 1998].

To drive the OGCM "OPA7," satellite-derived wind stresses are completed with water and heat fluxes. These fluxes are computed using bulk aerodynamic formulae with stress from ERS-1, *Reynolds and Smith*'s [1994] SSTs, and all other parameters derived from the atmospheric model Arpège-Climat [*Dequé et al.*, 1994] outputs. The OGCM has been forced from mid-1992 to 1995. Overall comparisons between the outputs of the ERS-1 forced OGCM, TAO in-situ data, and satellite observations have been performed for different ocean variables over the equatorial Pacific Ocean [*Grima et al.*, 1998]. Five-day outputs were analyzed spanning the 1992-1995 period, and during the specific period of FLUPAC and OLIPAC, linear interpolation of five-day outputs to daily values was performed for comparison with data.

2.4. The Coupled Biogeochemical Model

This OGCM is coupled to an off-line tracer nitrate model using the dynamical outputs to solve the advection-diffusion equations [*Levy*, 1996] on the OGCM grid:

$$\frac{\partial \mathrm{NO_3}}{\partial t} = -(\boldsymbol{u}.\nabla)\mathrm{NO_3} + K_h \Delta \mathrm{NO_3} + \partial_z\left(K_z \partial_z \mathrm{NO_3}\right) + \left(\frac{\partial \mathrm{NO_3}}{\partial t}\right)_{\text{biology}} \quad (1)$$

The left-hand term represents the eulerian variation of the tracer (nitrate) and is calculated as the sum of the advection terms (first term in the right-hand side), the horizontal diffusion terms (this one is quasi-negligible here), vertical diffusion terms, and the biological sink. Currents and diffusion coefficients are taken from the dynamical simulation. The last term represents the biological nitrate sink (biological model). As in the host physical model, the governing equations are solved on a C grid. An absolute requirement is that the biological tracer concentrations remain positive. Therefore a positive definite advection transport scheme [*Smolarkiewicz and Clark*, 1986] is used to compute advection.

Previous attempts to represent the biogeochemistry in the equatorial Pacific [*Toggweiler and Carson*, 1995 ; *Chai et al.*, 1996] were based on a biological model where the phytoplankton, the zooplankton, ammonium, and detritus were explicit compartments where the nitrogen fixed by photoautotrophs could accumulate. However, the field data and experimental knowledge to initialize these compartments and adjust the fluxes between each other are uncertain. Since we focus here on new production [*Dugdale and Goering*, 1967] we choose to reduce the ecosystem to a single nitrate compartment. Thus, in this simple system the new nitrate that is taken by the photoautotrophs cannot be stored in any compartment in the photic layer and must then be immediately remineralized at depth. This procedure presents the inconvenience of a too strict coupling between new production and remineralization that does not account for the natural storage into biomass or dissolved organic nitrogen and for the transport of stored nitrogen before remineralization. It was adopted, however, for its simplicity and ability to represent the variability of the nitrate field at the time of FLUPAC and OLIPAC.

New production is carried out by the phytoplankton, and thus its rate is biomass-dependent. It is also limited by the availability of light and nutrients. Limitation by light in our model is made according to *Kiefer and Mitchell* [1983]. The photosynthetic radiation incident at the surface is provided by the radiative flux used to force the dynamical model. Since our model does not include a phytoplankton compartment a special procedure had to be developed to estimate its biomass, or chlorophyll concentration, at a given place and time. The synthesis of the satellite Coastal Zone Color Scanner (CZCS) sea color data [*Yoder et al.*, 1993], as well as a 10 year monitoring experiment using ships of opportunity [*Dandonneau*, 1992], shows that the chlorophyll concentration at the surface decreases slowly from the eastern equatorial upwelling to the tropical waters to the north, to the south, or to the west (warm pool). Similarly, a large-scale decrease in the nitrate concentration and an increase in temperature are observed [*Chavez et al.*, 1996]. The FLUPAC and OLIPAC data also confirm that higher chlorophyll concentrations respond to higher nitrate concentrations. Given this, it is possible to derive an empirical linear relationship between the nitrate surface data and chlorophyll surface data (such a relationship was computed using the FLUPAC, OLIPAC, and the EqPac data) and to compute at each model time step the chlorophyll concentration at the surface. The vertical profile of chlorophyll is then rebuilt starting from the chlorophyll concentration at the surface propagated vertically via statistical equations by *Morel and Berthon* [1989]. Once a chlorophyll field is calculated, new production can be computed according to

$$\left(\frac{\partial NO_3}{\partial t}\right)_{\text{biology}} = -V_{\max}\frac{NO_3}{NO_3 + K_{NO3}}\frac{PUR}{PUR + K_E}[\text{Chl}] \tag{2}$$

where Vmax is the maximum nitrate assimilation rate (μmol NO_3 mg Chl^{-1} s^{-1}) and K_{NO_3} is the half saturation concentration (μmol NO_3 kg^{-1}). The Vmax and K_{NO_3} values which give the best fit with the FLUPAC and OLIPAC observations of nitrate concentration are 4×10^{-3} μmol NO_3 mg Chl^{-1} s^{-1} and 0.01 μmol NO_3 kg^{-1}, respectively. These parameters set a Michaelis-Mentens-type limitation to the nitrate sink according to *MacIsaac and Dugdale* [1969]. PUR is the photosynthetic usable radiation (mol photons m^{-2} s^{-1}) [*Morel*, 1991] deduced from the short wave downward radiation and a phytoplankton light absorption scheme based on a two wavelength (red and blue) light absorption spectrum (J. Ballé, personal communication, 1998). The daily cycle of irradiance is not represented in this model, and K_E (i.e., the half-saturation constant for PUR) is taken to be equal to 70×10^{-6} mol photon m^{-2} s^{-1} in order to reproduce a limitation by light in agreement with the results of light-photosynthesis experiments made by K. Allali and M. Babin during FLUPAC and OLIPAC [*Moutin and Coste*, 1996].

The parameters Vmax and K_{NO_3} which control this nitrate sink are the same over the basin as if a phytoplankton population with constant physiological properties occupied the studied area. This simplified representation of the biology in a domain which is nitrate-limited in the warm pool and subtropical gyres and nitrate-rich in the equatorial HNLC region does not disagree with the conclusions of *Landry et al.* [1997], who do not observe any fundamental difference in the characteristics of the phytoplankton populations between these two regimes. Using a unique set of constants for nitrate assimilation kinetics all over the basin can be justified by the fact that nitrate is not the primary limiting factor in the equatorial Pacific. In fact, iron limitation is effective everywhere [*Price et al.*, 1994]. As a consequence, nitrate fixation is mostly dependent on biomass, and limitation by nitrate occurs only when the nitrate concentration is less than K_{NO_3}.

The computation of the nitrate sink is made down to the depth of the photic layer. New production is then instantaneously exported as particles below the photic layer with an exponential decrease, and remineralized, as by *Honjo* [1978]. The constant for the exponential decrease of remineralization with depth was fixed to 120 m, a value which fits best with the sediment traps data from the EqPac cruises [*Murray et al.*, 1995].

The model was initialized on April 20, 1992, with nitrate concentrations from Levitus climatology. The initial nitrate field is clearly not in equilibrium with the large-scale dynamics of the equatorial Pacific at this time, especially in the surface layer (indeed, warm pool nitrate concentrations in the Levitus climatology are seemingly too high). In order to achieve equilibrium the biological model was spun up by rerunning a perpetual April 1992 to March 1993 year five times. After this 5 year spin up the nitrate field was in nearly equilibrium with the physics of the model, the integrated amount of nitrate in the photic layer increasing by only 3%

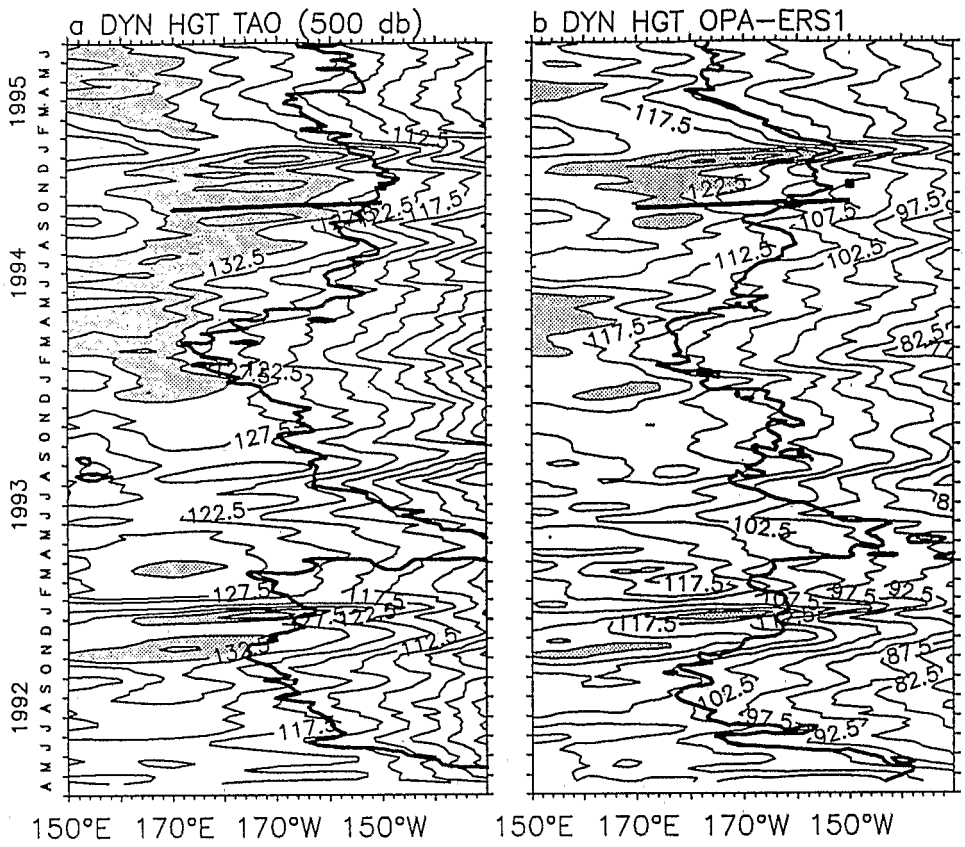

Figure 2. (a) Equatorial section of observed Tropical Ocean Global Atmosphere (TOGA)- Tropical Atmosphere Ocean (TAO) and (b) OPA-European Remote Sensing (ERS)-1 modeled dynamic heights. These dynamic heights are referenced to 500 dbar. Areas of pronounced dynamic height pulses are shaded. The 28°C observed isotherm [*Reynolds and Smith*, 1994] and the modeled 28°C isotherm are superimposed on Figures 2a and 2b, respectively. The FLUPAC equatorial transect is superimposed as a dark line in September-October 1994, and the OLIPAC cruise is represented by a dot at150°W in November 1994.

during the fifth year. The model was then forced with the 1992-1995 dynamical simulation, and results are then examined from mid-April 1992 to June 30, 1995. From 15° to 20°S and 15° to 20°N the modeled nitrate is smoothly relaxed to Levitus climatology. At the western and eastern boundaries a similar but stronger relaxation is imposed in order to remedy abnormally strong vertical advection of nitrate due to unrealistic vertical motions near America's and Papua New Guinea's coasts in the dynamical model. This procedure, however, did not affect the dynamic or biological nitrate fluxes at 165°E where the model results are compared to the observations. The biological model is active down to 1260 m depth where nitrate concentrations are relaxed to Levitus climatology.

3. Dynamical and Biogeochemical Fields: Data and Model Comparisons

3.1. The Equatorial Pacific in 1992-1995

An equatorial section deduced from TOGA-TAO and modeled dynamic heights (referenced to 500 dbar) is presented in Figure 2 together with the observed and modeled 28°C isotherm position for the period. The 28°C isotherm position is an indicator of the position of the eastern edge of the warm pool [*Picaut et al.*, 1996]. The equatorial section of the modeled dynamic height (Figure 2b) shows a -10 cm systematic mean bias with respect to the observations (Figure 2a). Reasons for this are unclear at present and merit further investigations. However, as in the observations, time varying features such as Kelvin pulses are in very good agreement.

The period from 1991 to 1994 is characterized by three successive weak warm events that resulted in a long-lived warm anomaly in the equatorial Pacific [*Goddard and Graham*, 1997]. During that time the Southern Oscillation Index (SOI) remained negative [*National Oceanic and Atmospheric Administration* (NOAA), 1994]. *Kessler and McPhaden* [1995] described the period 1991-1993 during which the U.S.-JGOFS EqPac cruises took place. Abnormally high temperature and low productivity representative of El Niño conditions prevailed during the spring cruise as can be seen here from the 28°C isotherm eastward positions (Figures 2a-2b). In contrast, the fall cruise was conducted when near normal conditions associated with a brief return of moderate easterlies were back [*Murray et al.*, 1995] as indicated by 28°C positions near the dateline both in data and model. From October up to December 1992, seasonal occurrences of westerly wind bursts were observed that are seen both in the data and the model to generate downwelling Kelvin waves. These propagate to the east in association with the warm pool eastward displacement. Then abnormally warm conditions came back in 1993, a weak El Niño period which seemed to

be more characteristic of a slightly enhanced seasonal cycle [*Boulanger and Menkes*, 1995]. After a brief return of moderate conditions in late 1993 and the beginning of 1994, warm conditions returned during the last semester of 1994. This last semester of 1994 was characterized by a series of westerly wind bursts [*Eldin et al.*, 1997]. The modeled variability is in very good agreement with the data both in terms of dynamic height and warm pool eastward displacement. During this time period the eastward shift of the warm pool was particularly pronounced, followed by a retreat of the warm pool position to the dateline during the first semester of 1995. This corresponded to weak cold conditions in the Pacific [*Goddard and Graham*, 1997].

These east-west oscillations of the eastern edge of the warm pool can be attributed to zonal advection by eastward currents [*Picaut et al.*, 1996]. During the FLUPAC and OLIPAC cruises this resulted in positive SST anomalies as high as 2°C [*NOAA*, 1994] in the central Pacific in October-November 1994. Associated with the warm pool displacement and the series of westerly wind bursts, a series of downwelling Kelvin waves that may have further contributed to the eastward shift of the warm pool [*Picaut and Delcroix*, 1995] were generated in September, in November, and in December 1994 when the FLUPAC and OLIPAC cruises took place.

The first one was partly generated by a westerly burst near 160°E in early September [*Eldin et al.*, 1997]. Following the September wave, a westerly wind event occurred in October [*Eldin et al.*, 1997] at the beginning of the FLUPAC equatorial transect. This pulse, however, did not generate any clear propagation of Kelvin wave signal in neither the TAO dynamic height (Figure 2a), the TOPEX/POSEIDON sea level anomaly (not shown), nor the model (Figure 2b). At that time the zonal current observed by the TAO ADCP mooring located at 165°E indicates westward flow down to a 100 m depth. Hence the downwelling wave may have been damped by the interaction with the surrounding flow in opposite (westward) direction to the wave-induced eastward current [*Brossier*, 1987; *McPhaden et al.*, 1986]. Another reason may be that a reinforcement of easterlies in the central Pacific, at that time, counteracted the genesis of the downwelling Kelvin wave. Then, in November, a marked westerly wind burst generated a clear downwelling Kelvin wave that propagated across the basin. The OLIPAC passage at the equator occurred while the Kelvin wave associated sea level was rising. Lastly, a strong westerly burst at the beginning of December 1994 forced a strong downwelling Kelvin wave and is observed propagating all the way to the eastern Pacific. It marks the end of Kelvin wave activity in the western Pacific (Figure 2) and of the eastward shift of the 28°C isotherm.

Remotely forced processes such as the downwelling Kelvin waves have been thought to affect the geochemical (nutrients) and biological (chlorophyll, primary production, plankton community structure) fields [*Murray et al.*, 1994; *Bidigare and Ondrusek*, 1996]. They also contribute to the zonal displacement of the eastern edge of the warm pool. Thus the FLUPAC and OLIPAC cruises sampled the ocean during a period of time that appears to be affected by major features of the large scale equatorial dynamics which characterize the equatorial Pacific.

3.2. Vertical Physical and Biogeochemical Structures During FLUPAC and OLIPAC

3.2.1. Cruises data. The meridional FLUPAC transect at 165°E first sampled the tropical waters of the Coral Sea in the south and then entered the warm pool waters (SST > 28°C) at ~10°S (Figure 3a). During this transect, conditions were close to the reference conditions described in *Radenac and Rodier* [1996]. The thermocline was rather diffuse as opposed to the halocline (Figure 3b) which was well marked and shallower than the thermocline and decoupled from it. This decoupling was particularly apparent at 4°S-2°N where a low-salinity core (<34.1 practical salinity unit (psu)), associated with the westward flowing South Equatorial Current (SEC), was found from the surface down to 100 m depth. At ~150 m depth, south of the equator, the high-salinity core (>34.9 psu) was characteristic of South Pacific waters of subtropical origin. The Equatorial Undercurrent (EUC) was well developed with a maximum speed of 50 cm s^{-1} at 175 m (Figure 3c). As is often observed at this longitude, the surface mixed layer was nitrate-exhausted all along this transect down to ~75 m, including the region close to the equator (Figure 3d). The nutricline closely followed the halocline, and the subsurface chlorophyll maximum (Figure 3e) that peaked at 0.5 μg L^{-1} was found at the nutricline depth as is commonly observed.

During the OLIPAC cruise the isotherms near the equator at 150°W showed the characteristic spreading indicating the presence of the EUC core at 150 m depth (Figures 4a and 4c). They slowly and gradually spread and deepened to the south as was previously described during the Hawaii-Tahiti shuttle experiment [*Wyrtki and Kilonsky*, 1984]. Around 150 m the high-salinity tongue originating from South Pacific subtropical waters (Figure 4b) penetrated from the south toward the equator. The core of the EUC had a maximum velocity of 70 cm s^{-1} (Figure 4c). Above it the flow remained eastward almost up to the surface. Farther south, currents were weak and mostly westward except around 10°S where an eastward flow was measured, as is occasionally reported in the central Pacific [*Eldin*, 1983; *Wyrtki and Kilonsky*, 1984; *Kessler and Taft*, 1987]. The observed distribution of nitrate (Figure 4d) was close to those previously described in the central Pacific [*Carr et al.*, 1992; *Wyrtki and Kilonsky*, 1984; *Murray et al.*, 1995]. The mixed layer was nutrient depleted south of 10°S. To the north, surface concentrations were similar to the values observed during the 1992 spring EqPac cruise characteristic of El Niño warm conditions [*Murray et al.*, 1994]. Corresponding to this nitrate structure, the chlorophyll distribution showed a deep chlorophyll maximum below the top of the thermocline in the southern part of the section and showed relatively high chlorophyll values (>0.25 μg L^{-1}) extending from 100 m up to the surface to the north (Figure 4e). This transition from an oligotrophic regime to a mesotrophic one has been previously described in the area between 130° and 140°W, where its latitude varied between 10° and 14°S [*Dandonneau and Eldin*, 1987].

Both at depth and at the surface the equatorial FLUPAC transect sampled two different physical regimes which are more extensively described by *Eldin et al.* [1997]. The boundary between these two regimes is best evidenced in Figure 5b which shows a sharp salinity front of ~0.8 psu near

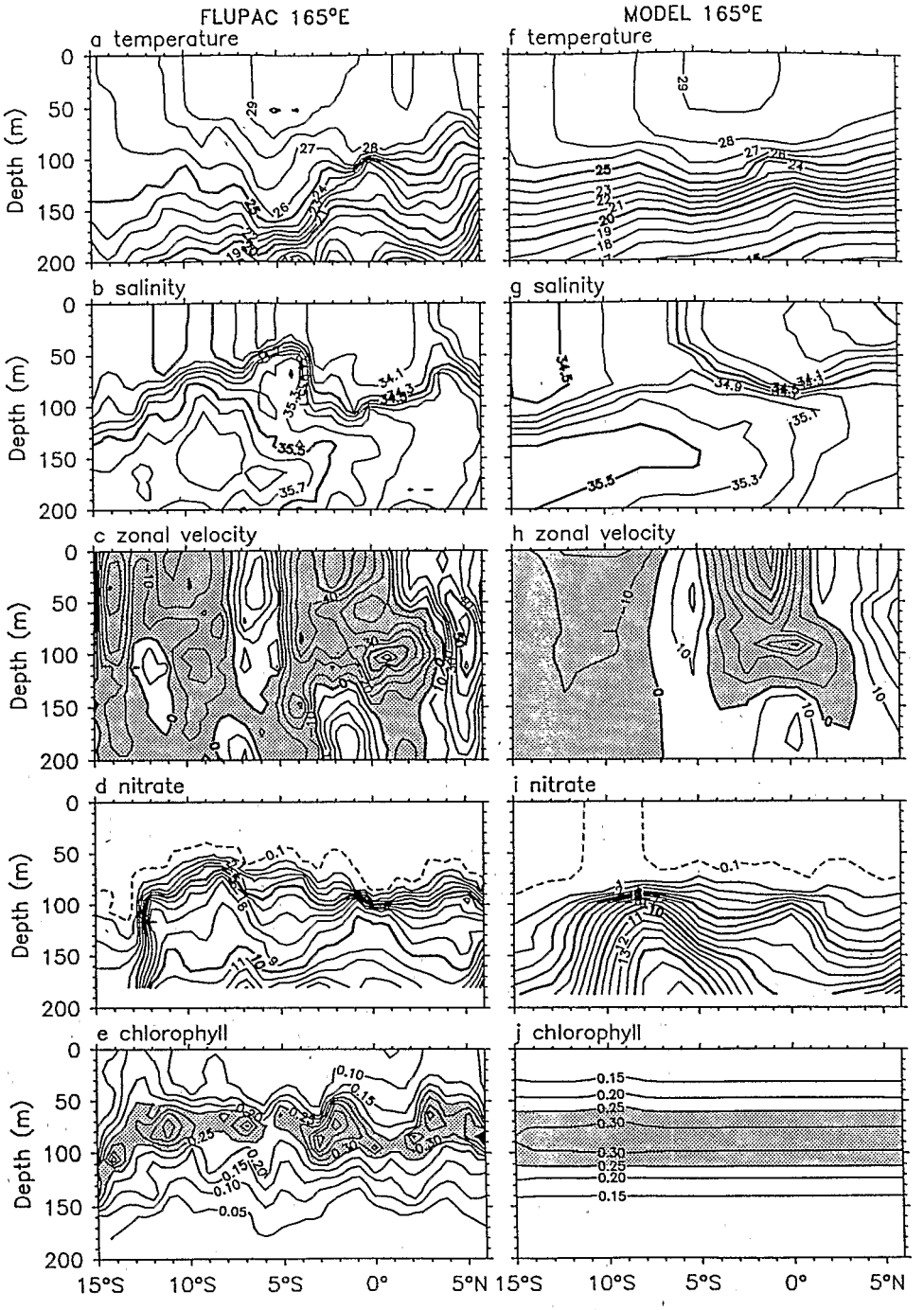

Figure 3. (a) Temperature (°C), (b) salinity (practical salinity unit (psu)), (c) zonal velocity (cm s^{-1}), (d) nitrate (μmole kg^{-1}), and (e) chlorophyll (μg L^{-1}) observed during FLUPAC along 165°E and (f-j) simulated by the OPA-ERS-1 model. Westward currents are shaded.

175°W. The fresh (<35 psu) and warm (29°-30°C) waters west of this front were characteristic of the warm pool waters with a salinity barrier layer above the thermocline [*Lukas and Lindstrom*, 1991], representing the continuity at depth of the east-west surface front. A well-marked thermocline was located between 100 and 125 m all along this transect (Figure 5a), and the absence of an east-west slope was characteristic of El Niño conditions [*Philander*, 1989]. The surface current (Figure 5c) showed a dominantly westward SEC except in the eastern part of the transect where the westward flowing SEC usually prevails [*Wyrtki and Kilonsky*, 1984; *Kessler and Taft*, 1987; *Eldin et al.*, 1997]. Nevertheless, surface current reversal has been commonly observed at this longitude, in springtime, during El Niño periods and/or associated with downwelling Kelvin waves [*Firing et al.*, 1983; *Kessler and McPhaden*, 1995]. The patch of eastward current, observed

near 175°W, was probably associated with the October westerly wind event [*Eldin et al.*, 1997]. At subsurface a strong westward current was situated right above the thermocline in the west. This type of structure, already observed west of the salinity front, has been interpreted as the response to a westerly wind forcing [*Kuroda and McPhaden*, 1993]. It can also be indicative of the dynamics associated with subduction of the SEC under the salinity barrier layer as explained by *Vialard and Delecluse* [1998a, b]. The EUC was located beneath and tilted upward toward the east. The distribution of chlorophyll concentration was consistent with the salinity distribution (Figure 5e): the salinity front separated chlorophyll poor waters in the warm pool from upwelling waters where chlorophyll was more abundant. At first sight this front similarly separated nitrate-exhausted water of the warm pool from the nutrient rich upwelling region (Figure 5d). However, one can note a spatial offset between nitrate-exhausted waters ($[NO_3]<0.1$ μmole kg^{-1}) and the salinity or chlorophyll front ($[Chl]<0.1$ μg L^{-1}) or zooplankton front (Figure 1). This offset was most probably controlled by biological processes in which nutrient removal by phytoplankton exhausted the nitrate dynamical supply near the barrier layer. The nitrate concentration increased eastward, reaching values >3 μmole kg^{-1} at 150°W. In the upwelled waters, consistent with the availability of nitrate in the upper well-lighted waters, the chlorophyll maximum was located in

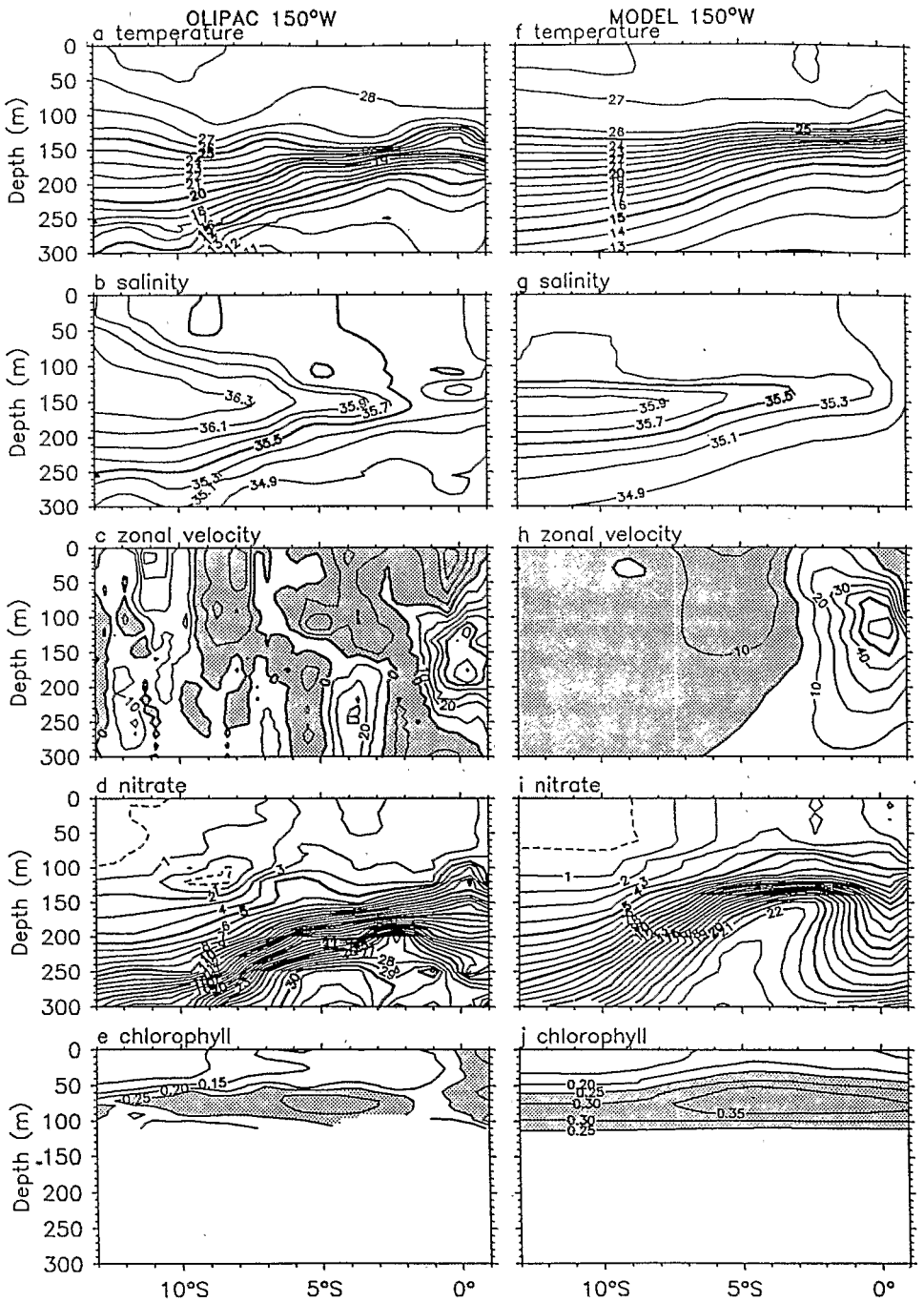

Figure 4. Same as Figure 3 but for the OLIPAC section along 150°W.

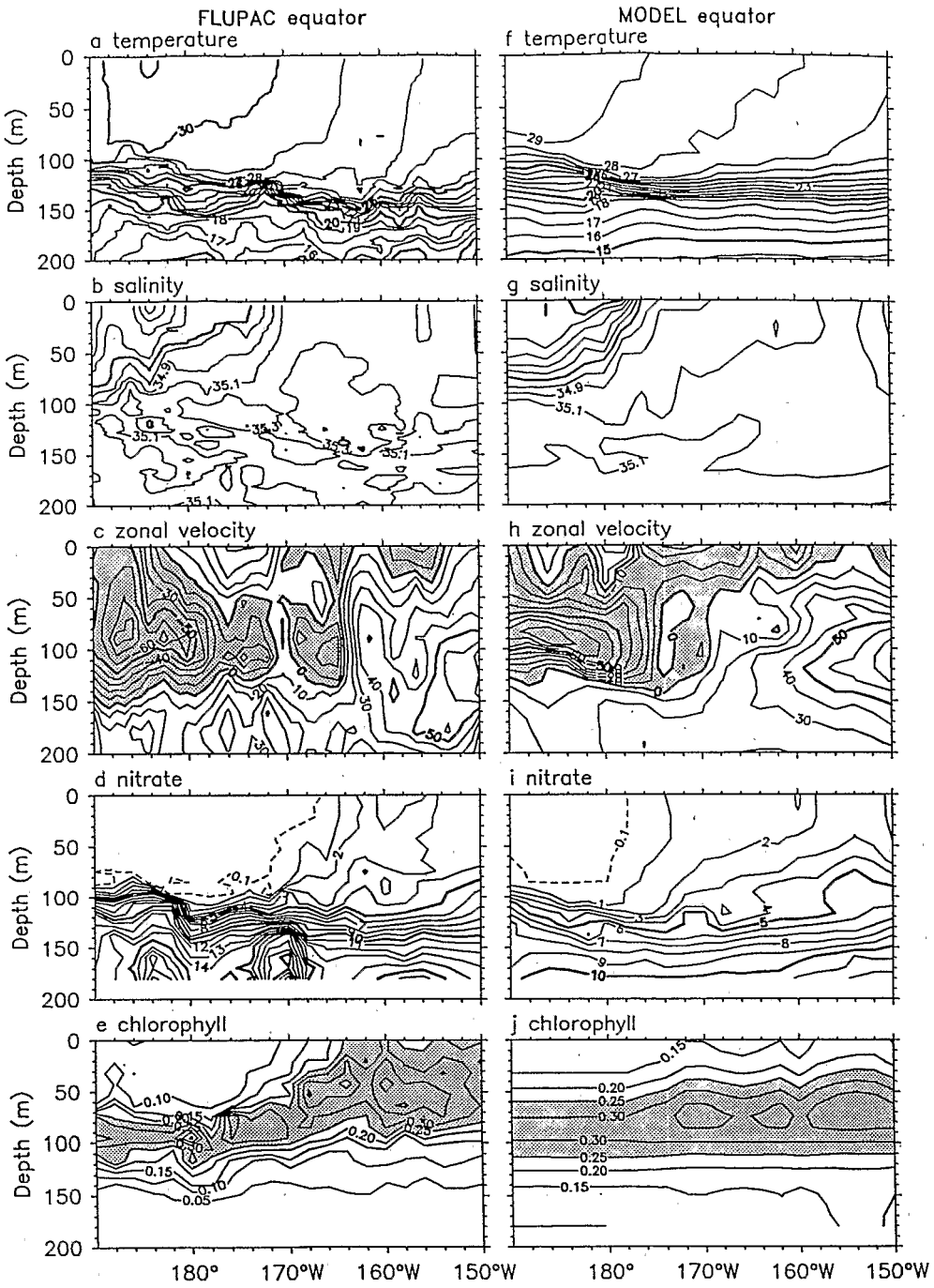

Figure 5. Same as Figure 3 but for the FLUPAC equatorial section.

the surface mixed layer. On the warm pool side a deep (80 m) chlorophyll maximum was positioned just below the salinity barrier layer at the top of the nutricline. The chlorophyll concentration in the deep maximum was ~0.30 μg L^{-1} and was similar to that found in the upwelled waters farther east. In terms of biomass per square meter, however, the upwelled waters were richer than the warm pool waters because the chlorophyll rich layer was thicker there (see also section 4). Hence the FLUPAC equatorial data highlighted one of the most remarkable features of the equatorial Pacific: the warm, fresh, and oligotrophic waters of the western Pacific warm pool are separated by a sharp salinity front from the colder, saltier, and mesotrophic waters of the upwelling waters. These two contrasted regimes are also evidenced in the upper trophic levels such as zooplankton distribution (Figure 1).

3.2.2. Model results. At 165°E, modeled temperatures are generally in good agreement with the data at the same depth (Figure 3f). However, the model temperature shows less spatial structure than the data, and in particular, it fails to reproduce the spreading of isotherms in the core of the EUC. The fresher water (<34.1 psu) in the equatorial region is correctly simulated although the surface front south of 4°S is more intense than in the observations (Figure 3g). The modeled EUC is much weaker than the observed (Figure 3h).

This discrepancy explains the lack of spreading of the isotherms in the modeled temperature. It has to be noted that the modeled current structures are much simpler than the observed and that countercurrents are generally too weak in this simulation.

At 150°W, thermohaline structures are generally well reproduced, but there are systematic biases such as colder temperatures in the upper layers and fresher waters in the salinity field. Zonal velocity shows patterns that are too smoothed (Figures 4c-4h) as compared to data and do not present any current variability south of 5°S. It has also to be stressed that the EUC core is too shallow.

In contrast, the equatorial transect is quite well simulated. The temperature distribution is good despite a 1°C bias in the upper layer waters (Figure 5f). The salinity field (Figure 5g) is well simulated. In particular, the salinity zonal gradient and its location are well reproduced. Being able to correctly simulate this gradient is crucial as it was seen to separate two different regimes. In the western part of the equatorial transect the EUC is weaker in the model than in the data and tilts upward toward the east where both data and model agree better (Figure 5h).

Considerations about dynamical simulations of these three particular transects are consistent with the more general conclusions of *Grima et al.* [1998]: the EUC core and the thermocline depth are shallower in the model than in the data, and the thermocline is generally too diffuse (as most modeled thermocline) and the countercurrents are too weak in the model.

In the oligotrophic region (warm pool), at 165°E, the surface NO_3 depletion (Figure 3i) is deeper than the observed and the nutricline tends to be too diffuse compared to observations. This can drive significant differences between observations and model outputs below the mixed layer. Reasons for this are certainly various. Among those the tendency of the model to have a too diffuse pycnocline structure can be invoked, as the nutricline is, at first order, shaped by the pycnocline structure in observations [*Radenac and Rodier*, 1996]. Discrepancies between the data and model due to limitations of the biological nitrate sink will be evoked later in the text.

At 150°W, the upper layer NO_3 concentrations are reasonable, and the transition between nutrient poor ($[NO_3]<0.1$ μmole kg^{-1}) and nutrient rich waters is fairly well reproduced (Figure 4i). At depth, obvious biases show up such as a too shallow nutricline. It is hard to understand what factors control these biases in such complex 3-D dynamics. However, some of the spurious nutrient trapping near the surface may be related to the lack of horizontal transport of organic nitrogen as evoked in the model description [*Najjar et al.*, 1992; *Bacastow and Maier-Reimer*, 1991]. In the equatorial region the simulated nitracline shows a weaker than observed doming associated with the EUC core. This lack of structure is obviously related to the simulated EUC that is too shallow compared to the data (Figures 4c-4h).

Along the equator the surface transition between nutrient poor (oligotrophic) and nutrient rich (mesotrophic) waters is correctly simulated (Figure 5i). In the model this surface transition in the nitrate field is totally correlated to the salinity front at that period of time (see section 4). Therefore, if the offset seen in the data between the salinity front and nitrate-exhausted waters is indeed related to biological activity, our simple nitrate sink model does not reproduce this process. At depth, however, this transition is found at the bottom of the barrier layer, as in the data, which indicates that processes maintaining the depth of the poor pool differ from those maintaining the barrier layer. Underneath the photic layer the nutricline is too diffuse compared to the data.

The chlorophyll values, which are statistically computed in the model, show higher surface concentrations and a much smoother pattern than are in the observations (Figures 3j, 4j, and 5j). This is not surprising as the statistics used here have been derived globally and thus cannot account for local variations as observed along the transect. The position and values of the deep maximum chlorophyll are rather well captured by the statistics. In the mesotrophic region, modeled chlorophyll is generally 30%-40% too high compared to observations but the deep chlorophyll maximum is well located (Figures 4j and 5j).

The validations of the coupled dynamical-biogeochemical conditions along the FLUPAC and OLIPAC transects have shown that despite imperfections the model is able to reproduce the major observed features at specific locations and times with good qualitative agreement. In particular, one important aspect and one merit of these simulations are that they are able to reproduce the two contrasted regimes of the equatorial waters.

4. The Modeled New Production

4.1. Modeled New Production at the Equator From 1992 to 1995

The variability of temperature and salinity distributions, currents, and dynamic topography of the model outputs is in good agreement with TAO buoy observations over 1992-1995 (see above and *Grima et al.*, [1998]), and the modeled nitrate field is also reasonable compared to the observations (see above). This allows us to investigate further the large-scale equatorial features of coupled conditions during 1992-1995 as given by the simulations. Figure 6 shows the equatorial section of modeled sea surface salinity (SSS), zonal currents, and new production. The succession of westward and eastward zonal currents is responsible for the zonal displacement of the eastern edge of the warm pool and fresh pool (SSS<34.8 psu). The mechanisms creating these east-west migrations are detailed by *Picaut et al.* [1996] and by *Delcroix and Picaut* [1998]. Thus the warm/fresh/poor pool region is moved east and west according to the large-scale ENSO-related zonal current.

In this model output (Figure 6) the well-marked salinity front (Figure 6a) that separates the fresh warm pool to the west from the upwelling region moves eastward and westward and is displaced by the zonal currents (Figure 6b). Strong pulses of eastward velocities are shown to be associated with the occurrences of downwelling Kelvin waves such as those of November-December 1992 and 1994. The SSS front is seen to be particularly pronounced during these events when current convergence at the front is particularly strong. The last semester of 1994 is the longest period when the zonal current is mostly eastward. This causes the front and the eastern edge of the warm pool (position of the 28°C isotherm) to gradually move eastward and to sharpen. When eastward currents are not so strong or westward currents occur, the salinity front is

more diffuse (Figures 6a and 6b) [*Vialard and Delecluse*, 1998a, b].

Primary production allows us to differentiate between the equatorial poor and rich regimes (Figure 6c). Figure 6c clearly shows that during the 1992-1995 period, two distinct regimes prevailed that are characteristic of the warm pool (poor pool) region on one side and the upwelling region where waters are richer on the other side. These two regimes are separated by a "primary production front" that is closely related to the salinity front (see the position of the 34.8 psu isohaline and the primary production front on Figure 6c). Only during the first three months of the simulation, a decoupling between the new production and salinity front occurs. This time period should be considered with caution in the simulation as it is close to the ending of the 5 year spin up calculated with a perpetual April 1992 to March 1993 year. Note that the relation between the primary production front and the eastern edge of the warm pool is particularly strong when the salinity front is well marked, in November-December 1992 and during the last semester of 1994, and closely follows the displacements of the salinity front. The FLUPAC and OLIPAC cruises sampled this last episode.

As seen in Figure 5, observed nitrates at the time of FLUPAC closely reflect the position of the simulated primary production (nitrate) front which is therefore displaced via zonal advection during the period of interest. Additional data from November-December 1994 [*Inoue et al.*, 1996] show that the modeled front position is also in agreement with observations at that time. The variables recorded along the equator during FLUPAC further confirm that the front actually separates the oligotrophic warm pool region from a mesotrophic regime east of the front (Figure 1). Consequently, primary production can vary greatly during El Niño or La Niña periods because of these large east-west displacement patterns of the warm pool. For example, it was greatly reduced during late spring of 1992, at 140°W, in agreement with the observations made during the EqPac spring cruises [*Murray et al.*, 1995]. However, further simulations of the ENSO cycle are required to really estimate primary production reduction when strong El Niño occurs. In particular, spectacular impacts of the 1997-1998 El Niño should give further insights on such reductions.

4.2. Comparison Between the Warm Pool and the Upwelling Regimes

Given the clear separation between the regimes, it is useful to introduce the NINO4 (160°E-150°W, 5°S-5°N) and NINO3 (150°-90°W, 5°S-5°N) boxes often used to contrast two dynamical (warm pool and upwelling) regions for ENSO-related issues [*NOAA*, 1994]. Indeed, during the 1992-1995 time period one can see that these two regions correspond to the warm pool region (NINO4) and the upwelling region (NINO3). Averaged primary production amounts to ~0.9 mmol NO_3 m^{-2} d^{-1} in NINO4 and 2.1 mmol NO_3 m^{-2} d^{-1} in NINO3. These can be thought of as representative of mean conditions during this weak ENSO period for the two regimes.

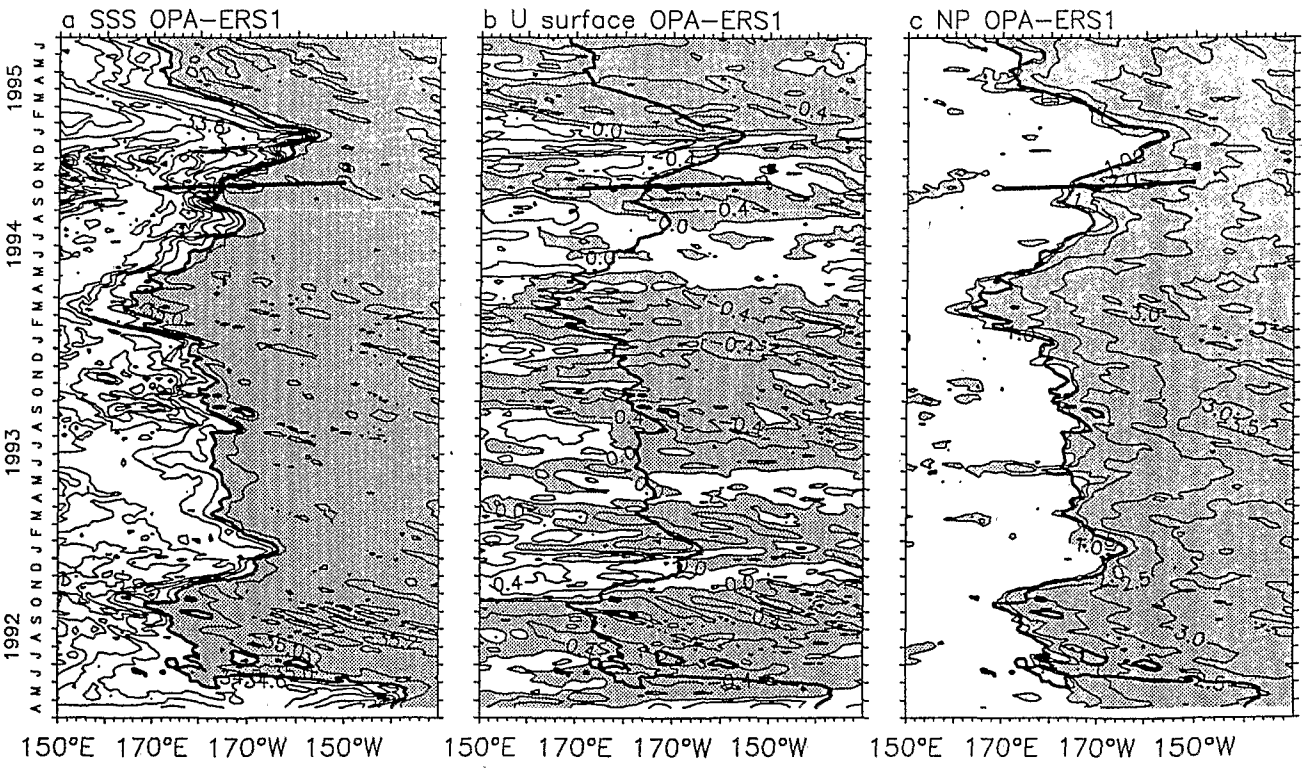

Figure 6. OPA-ERS-1 model outputs along the equator for the whole simulation: (a) salinity (psu), (b) zonal velocity component (cm s^{-1}), (c) new production (mmol NO_3 m^{-2} d^{-1}). Sea Surface Salinity (SSS) > 34.8 psu, westward currents, and new production > 1 mmol NO_3 m^{-2} d^{-1} are shaded. The 34.8 psu isohaline marking the SSS front is superimposed on Figures 6a-6c. The FLUPAC equatorial transect is superimposed as a dark line in September-October 1994, and the OLIPAC cruise is represented by a dot at 150°W in November 1994.

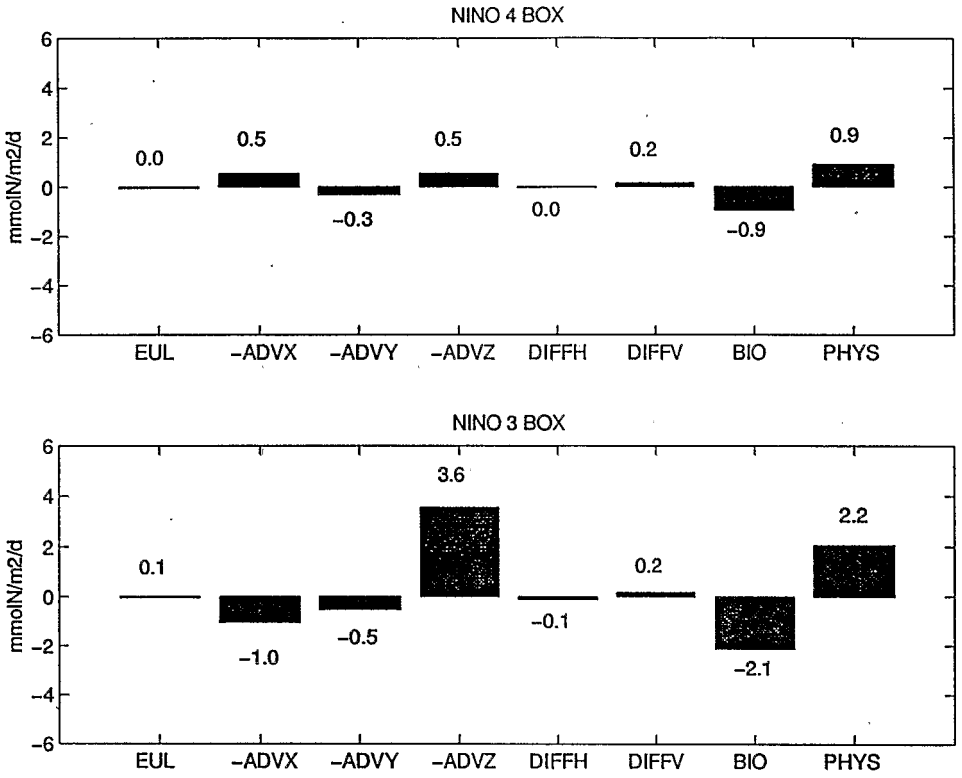

Figure 7. Budgets of nitrate terms of (1) integrated from the surface down to the euphotic layer depth in the NINO3 and NINO4 boxes for the 1992-1995 simulation. -ADVX, -ADVY, -ADVZ are the zonal, meridional and vertical advection terms; DIFFH and DIFFV are the contributions of horizontal and vertical diffusion terms; BIO is the nitrate sink (new production) and PHYS = -(ADVX + ADVY + ADVZ) + DIFFH + DIFFV. The eulerian term EUL = PHYS + BIO

So far, model simulations are the only way to seize the large-scale primary production variations as shown above. The model further allows us to understand the dynamics underlying the regimes that are observed. We have stressed the contrast between the warm/fresh/poor and cold/salty/rich equatorial regimes, and we can now estimate the budgets that lead to these two contrasted regimes. Budgets of nitrate integrated from the surface down to the euphotic layer depth are calculated in the NINO4 and NINO3 boxes by integrating (1) over the photic layer. This gives a representation of the respective roles of biology and the dynamics for the control of nitrate of the photic layer.

Figure 7 shows the relative contribution of all terms in the vertical integration of (1) for NINO4 and NINO3 boxes. The last histogram bar sums up the contribution of all the advective and diffusive terms and thus represents the physical forcing. In each case, eulerian terms are nearly zero so that one can understand the distribution of nitrate as a sum of dynamical effects and biological uptake. In the warm and poor pool region (NINO4), the supply of nitrate is mainly due to horizontal advection by the SEC (not shown here) that brings nitrate richer waters from NINO3 region and to upwelling of richer waters from beneath the photic layer, which in that region roughly corresponds to the nitracline depth. Some losses are conveyed by meridional divergence. This all amounts to a new primary production that is ~0.9 mmol NO_3 m^{-2} d^{-1}. As expected, the NINO3 region is much more dynamical, and production is much higher. Contrary to NINO4, the dominant physical forcing is vertical advection of richer waters from the EUC core (not shown here) which confirms the results given by *Chai et al.* [1996] at 0°,140°W. This upwelling of the nitrate effect is somewhat counterbalanced by meridional divergence and loss of nitrate to the west by horizontal advection. This analysis illustrates the variety of processes that control nitrate concentrations and shows that the coupling between biology and physics can only be envisioned in a 3-D way.

4.3. Comparison With Other Results

At this point it is worth saying that our simple biological sink with constant *V*max and K_{NO_3} parameters is able to reproduce the major features of such two different regimes as the warm pool and upwelling regimes. The simplicity of the biogeochemical model adopted in this work is based on the empirical nitrate-chlorophyll linear relationship. In earlier versions of the model in which the nitrate sink was computed without chlorophyll it proved impossible to correctly reproduce the nitrate field observed during FLUPAC and OLIPAC. It must, however, be recognized that there is no objective reason why the nitrate-chlorophyll relationship at the surface should be linear. The correlation between these two variables is low. The lack of correlation partly arises from the chlorophyll measurements that are affected by a relatively important instrumental error (filtration, pigments extraction, acidification step, etc.) and by short-term variability. Modern data are rare, and ancient data suffer from intercalibration problems. This dispersion prevents us from finding out in the

data a more comprehensive nitrate-chlorophyll relationship. The assumption that chlorophyll at the surface is linearly and positively related to nitrate is certainly not valid everywhere in the equatorial Pacific. For instance, in the eastern Pacific the surface waters with high NO_3 (and Fe) content brought up to the surface by the upwelling have a low chlorophyll content at the source of the upwelling, which then grows up very quickly while NO_3 decreases. Nevertheless, most of the equatorial Pacific is occupied by phytoplankton populations dominated by the picoplankton [*Blanchot et al.*, 1992] and seems to respond to the environment like an oligotrophic ecosystem, whatever the nutrient-exhausted waters or the HNLC waters are considered [*Landry et al.*, 1997]. This relative uniformity of the equatorial Pacific makes it reasonable to use a single relationship to estimate the chlorophyll at the surface using nitrate concentration, and the existing information only permits us to use a linear relationship. It has also been noted that the statistical and the observed chlorophyll fields were not in agreement in some parts of the studied domain. The effect of these discrepancies on the adjusted nitrate sink caused by photosynthesis should be small because the bias itself is relatively small and because it occurs at depths where only 1%-10 % of incident light penetrates, so that the error on integrated new primary production is only a few percent. Thus, in spite of many subtleties that the simple model obviously cannot account for, the biological sink, as modeled, allows us to investigate the new production in the photic layer of the warm pool and of the upwelled waters.

The Vmax and K_{NO_3} values which give the best fit with the FLUPAC and OLIPAC observations of nitrate concentration are 4×10^{-3} μmol NO_3 mg Chl^{-1} s^{-1} and 0.01 μmol NO_3 kg^{-1}, respectively. These values are not directly comparable to observations made during FLUPAC an OLIPAC, where only the in situ incorporation of $^{15}NO_3$ at ambient NO_3 concentration was measured and not the kinetics of NO_3 assimilation. It is possible, however, to compare the biological sink of nitrate, i.e., new production, computed by the model to the NO_3 assimilation measured during the cruises and integrated over the photic layer. The nitrate taken up by photosynthesis in the model at the equator from 1992 to 1995 is shown on Figure 6. The values integrated from the surface to the bottom of the photic layer are <1 mmol NO_3 m^{-2} d^{-1} in the oligotrophic warm pool and between 2 and 3 mmol NO_3 m^{-2} d^{-1} at 0°, 150°W in the nitrate rich, upwelled waters east of the salinity/nitrate/chlorophyll front.

The measurements using $^{15}NO_3$ made during FLUPAC at 0°, 167°E (oligotrophic warm pool) show that nitrate fixation was ~1 μmol NO_3 m^{-3} h^{-1} from the surface to 100 m depth, which represents ~1.2 mmol NO_3 m^{-2} d^{-1} for a 12 or 24 hour period. (*McCarthy et al.* [1996] indeed observed that most of the nitrate assimilation occurs during the daylight period.) During OLIPAC along 150°W the average of nitrate assimilation measurements made south of 10°S (oligotrophic south Pacific subtropical gyre), both along the transect and during the fixed station at 16°S, was 0.74 mmol NO_3 m^{-2} d^{-1} [*Moutin and Coste*, 1996], very similar to the average determined from the warm pool while under a different regime (less sharp pycnocline and weaker vertical shear of current). The $^{15}NO_3$ uptake experiments made during the EqPac cruises at latitudes >6° (off the equatorial upwelled waters) range between 0.2 and 1 mmol NO_3 m^{-2} d^{-1} [*McCarthy et al.*, 1996]. Considering that the diffusion of colder, nitrate rich water through the 26°C isotherm should equilibrate the heat flux from the atmosphere into the ocean, in the domain defined by SST > 26°C (i.e., the warm pool), *Peña et al.* [1994] estimated that new production in this domain was on average 15 g C m^{-2} y^{-1}. Assuming that nitrate and carbon assimilation follows the C:N = 6.6 Redfield ratio, this amounts to a new production equal to 0.52 mmol NO_3 m^{-2} d^{-1} which is in rather good agreement with the above measurements and with the values given by our model.

In the nitrate rich upwelled waters at 0°, 150°W, nitrate fixation measured during FLUPAC in late October amounted to 3 mmol NO_3 m^{-2} d^{-1}, a value greater than that obtained at 5°S, 150°W during OLIPAC in November: 1.4 mmol NO_3 m^{-2} d^{-1} [*Moutin and Coste*, 1996]. The decrease in the nitrate concentration between the two cruises, consecutive to the strengthening of El Niño conditions, is an explanation for this relatively low value. The front between the warm pool and the upwelled waters indeed shifted rapidly to the east in October and November 1994 (Figure 6), inducing a rapid decrease of new production at 150°W. During the EqPac cruises, nitrate fixation was more intense at the equator (2°N-2°S) than at higher latitudes and averaged to 0.7 mmol NO_3 m^{-2} d^{-1} during the spring cruise, dominated by El Niño conditions, versus 2.8 mmol NO_3 m^{-2} d^{-1} in the autumn, when upwelling conditions re-established [*McCarthy et al.*, 1996]. These fall values are in agreement with the model results (Figure 6), but the model overestimates new production during the spring cruise. However, modeled new production at that time should be taken with care as is previously explained in paragraph 4.1. Thus, in the model the nitrate fixation integrated over the photic layer which generates a nitrate field that fits best with that observed during FLUPAC and OLIPAC is in agreement with the measurements made during FLUPAC and OLIPAC using ^{15}N experiments and during the EqPac fall cruise.

Large-scale estimates made for the 90°-180°W, 5°N-5°S domain are listed in Table 1. *Chavez and Barber* [1987]

Table 1. Estimates of New Production in the Equatorial Pacific Upwelling Region: 90°W-180°, 5°N-5°S

Origin	Estimate mmol NO_3 m^{-2} d^{-1}
Chavez and Barber [1987] using primary production and an f ratio of 0.44	2.7
F. Chai et al. [1996] using ecosystem model in the upper 120 m	2.3
Ku et al. [1995] using the ^{228}Ra budget in the euphotic zone (EqPac)	2.5
Toggweiler and Carlson [1995] using an ecosystem model	3.3
This study during 1992-1995 using the model	2.3

estimated that the 5°S-5°N zone, east of the dateline (i.e., the "equatorial cold tongue" [*Wyrtki*, 1981]), could support a yearly new production of 0.8 gigatons of carbon during normal conditions, which represents 2.7 mmol NO_3 m^{-2} d^{-1}. *Ku et al.* [1995] estimated a new production of 2.5 mmol NO_3 m^{-2} d^{-1} during the 1992 El Niño period. New production in the equatorial Pacific has also been estimated by 3-D coupled physical-biogeochemical models. Using average seasonal winds and heat forcings, *Toggweiler and Carson* [1995] found that the average new production in the 5°N-5°S, 90°-180°W area is 41.9 10^4 mol NO_3 s^{-1}, i.e., 3.3 mmol NO_3 m^{-2} d^{-1}. A similar model estimate by *Chai et al.* [1996], using an average seasonal forcing, amounts to 2.3 mmol NO_3 m^{-2} d^{-1}. Another 2-D modeling approach by *Carr et al.* [1995], based on the physical observations during the Wecoma cruise in 1988 (La Niña conditions), leads to an estimate of 4.4 mmol NO_3 m^{-2} d^{-1} in the central equatorial Pacific. Our estimation of new production in the same region is 2.3 mmol NO_3 m^{-2} d^{-1}. Considering that the 1992-1995 period was affected by warm conditions, our estimation of 2.3 mmol NO_3 m^{-2} d^{-1} should be considered as representative of El Niño conditions.

Such low values imply that the residence time of nitrate in the surface mixed layer is very long. Dividing the nitrate content of the mixed layer by the daily nitrate assimilation rate, *McCarthy et al.* [1996] found that the time required to deplete the mixed layer was of the order of 300 days. This long residence time is certainly a consequence of overall iron limitation in the region [*Martin*, 1990; *Barber*, 1992; *Price et al.*, 1994]. The same computation here (based on the nitrate content of the euphotic zone during FLUPAC at 0°, 150°W, i.e., 300 mmol m^{-2}, and new production in the model, equal to ~2.3 mmol m^{-2} d^{-1}) gives a residence time of the order of 130 days. In fact, the residence time should be even longer in our model because nitrate assimilation in the photic layer decreases the nitrate concentration at the surface, hence decreasing the prognostic chlorophyll at the sea surface and the vertical profile of chlorophyll in the photic layer computed according to *Morel and Berthon* [1989] and finally reducing new production. One can reasonably assume that the evolution of the mixed layer at sea follows a similar scheme. In addition, this crude computation ignores the vertical diffusion of nutrients through the pycnocline, which slowly but permanently refuels the mixed layer. Timescales to consume all the nitrate in the surface mixed layer of the equatorial Pacific should thus be of the order of 150-200 days, or even more, and this long duration is to be considered when examining the consequences of El Niño events on the primary production in the region: once El Niño conditions have settled, the nutrients upwelled during the previous La Niña episode can still fuel the new production of the equatorial Pacific for several months.

5. Conclusion

The equatorial Pacific presents two contrasted dynamical regimes: warm and fresh waters of the warm pool separated by a salinity front from the colder and saltier waters of the upwelling region. In this paper we have coupled the OPA-LODYC OGCM forced by ERS-1 winds to a nitrate transport model with a simple biological sink to estimate new production on large temporal and basin scales during the 1992-1995 weak El Niño. During the 1994 weak warm event the FLUPAC and OLIPAC French JGOFS cruises took place in the central and western equatorial Pacific.

These cruises sampled the equatorial Pacific when the warm pool was displaced eastward to ~160°W. This shift was characterized by the in-phase displacement of a salinity, nitrate, and chlorophyll front which separated two contrasted regimes: the oligotrophic warm pool waters to the west from the nitrate rich mesotrophic waters to the east. Consequently, the biomass observed, in terms of chlorophyll concentration, as well as the nitrate concentration in the photic layer to the east of this front were abnormally low, and biological fluxes were smaller than those observed on other cruises.

The best fit between modeled and observed nitrates gives a maximum speed of nitrate assimilation equal to 4 10^{-3} µmol NO_3 mg Chl^{-1} s^{-1} and a very low semisaturation constant (0.01 µmol NO_3 kg^{-1}) for the Michaelis-Menten function used in the sink. Given this and owing to a good agreement between the observed and modeled physical parameters, the coupled model reproduces a nitrate field for this period that is in rather good agreement with the nitrate concentrations measured both in the oligotrophic warm pool and the upwelling water. In particular, it is successful in simulating the transition between the two regimes. This allows us to place the FLUPAC and OLIPAC cruises into a larger-scale context and to examine the coupled physical-new production features of the 1992-1995 years with confidence.

During the 1992-1995 period the warm pool is shown to be associated with new production lower than 1 mmol NO_3 m^{-2} d^{-1} on average. This poor pool is separated from the richer waters of the upwelling (new production of ~2.3 mmol NO_3 m^{-2} d^{-1} in *Wyrtki*'s [1981] box) by a sharp new production front that is closely related to the sharp simulated salinity front. Such new production values agree with previous observational estimates. Such low values in the upwelling region can be considered as representative of weak El Niño conditions.

The salinity front at the eastern edge of the warm pool is subject to large zonal displacement in relation to ENSO-related zonal currents. Similarly, the transition between poor and rich waters experiences such huge zonal displacements due to zonal advection processes. In particular, when these fronts are displaced eastward in relation to El Niño eastward currents, new production can experience dramatic decreases. During the FLUPAC and OLIPAC cruises, new production was indeed low which can mainly be attributed to this eastward displacement of the poor pool. New production was also weaker than that measured 2 years earlier during the EqPac fall cruises along 140°W, during non-El Niño conditions, when the poor pool is shown to have retreated back.

This model has obvious flaws that reside in the oversimplification of the biological component. For instance, it was shown that nutrient trapping occurred in the east at depth. One way to improve that bias is to add a compartment of dissolved organic nitrogen in order to account for the horizontal transport of new production [*Stoens et al.*, 1998] rather than instantaneously remineralizing the whole production into particulate matter [*Najjar et al.*, 1992].

However, this model is a powerful tool for exploring the consequences of the strong coupling of the equatorial dynamics with biogeochemistry and biology of higher trophic

levels on seasonal to interannual time scales. For instance, other simulations are underway in order to reproduce strong El Niño and La Niña situations. So far, La Niña-related biological implications have been rarely observed [*Radenac and Rodier*, 1996] and will be assessed within the model context. Moreover, Figure 1 has shown that at the FLUPAC time the transition between the two regimes also corresponded to a sharp transition in CO_2 outgasing. Study is underway to couple this nitrate model to a carbon model in order to assess the global budgets and mechanisms of CO_2 fluxes to the atmosphere that are at work in the two contrasted warm pool and upwelling regimes. Such models with a simple physical-biogeochemical coupling have already proved successful in simulating the major nitrate trends and patterns as well as the major CO_2 fluxes in the equatorial Atlantic Ocean [*Thomas*,1995; *Loukos*, 1995]. Finally, our modeled new production can be used in successfully simulating the position of tuna forage in the western Pacific [*Lehodey et al.*, 1998] which experiences large east-west migrations in relation to ENSO [*Lehodey et al.*, 1997].

Acknowledgments. The FLUPAC and OLIPAC cruises were a contribution to the JGOFS international study of the equatorial Pacific and were coordinated by JGOFS-France. Financial support was given by Institut Français pour l'Exploitation de la MER (IFREMER), by Institut National des Sciences de l'Univers (INSU) and by Institut Français de Recherche pour le Développement en Coopération (ORSTOM). Ship time was ensured by GENAVIR/IFREMER. We are grateful to the captain and crew of R/V l'Atalante for generous and efficient help during the cruise. We are also grateful to C. Bournot, J.-Y. Panche, and F. Gallois, who took care of the equipment and ensured the high quality of the CTD data. M. Rodier, S. Bonnet, and P. Gérard made the measurements of nutrients, and the chlorophyll measurements presented here have been made by P. Conan and by A. Le Bouteiller. Comments from A. Le Bouteiller and R. Le Borgne are greatly appreciated. We are indebted to M. McPhaden for fruitful comments. Finally, we thank both reviewers whose comments greatly improved our first manuscript.

References

Bacastow, R., and E. Maier-Reimer, Dissolved organic carbon in modelling new production, *Global Biogeochem. Cycles, 5*: 71-85, 1991.

Barber, R. T., Introduction to the WEC88 cruise: An investigation into why the equator is not greener, *J. Geophys. Res.*, *97*, 609-610, 1992.

Barber, R. T., and F. P. Chavez, Biological consequences of El Niño, *Science*, *222*, 1203-1210, 1983.

Bentamy, A., Y. Quilfen, N. Grima, F. Gohin, M. Lenaour, and J. Servain, Determinations and validation of average wind fields from ERS-1 scatterometer measurements, *Global Atmos. Ocean Syst.*, *4*, 1-29, 1996.

Bidigare, R. R., and M. E. Ondrusek, Spatial and temporal variability of phytoplankton pigment distributions in the central equatorial Pacific Ocean, *Deep Sea Res., Part II*, *43*, 809-833, 1996.

Blanchot, J., M. Rodier, and A. Le Bouteiller, Effect of El Niño Southern Oscillation events on the distribution and abundance of phytoplankton in the western Pacific tropical ocean along 165°E, *J. Plankton Res.*, *14*, 137-156, 1992.

Blanke, B., and P. Delecluse, Variability of the tropical Atlantic Ocean simulated by a general circulation model with two different mixed layer physics, *J. Phys. Oceanogr.*, *23*, 1363-1388, 1993.

Boulanger, P., and C. Menkes, Propagation and reflection of long equatorial waves in the Pacific Ocean during the 92-93 El Niño, *J. Geophys. Res., 100*, 25,041-25,059, 1995.

Brossier, F., Numerical modelling of equatorial waves in the presence of a mean current, *J. Phys. Oceanogr.*, *17*, 1100-1113, 1987.

Busalacchi, A. J., M. J. McPhaden, and J. Picaut, Variability in equatorial Pacific sea surface topography during the verification phase of the TOPEX/POSEIDON mission, *J. Geophys. Res.*, *99*, 24,725-24,738, 1994.

Carr, M.-E., N. S. Oakey, B. Jones, and M. R. Lewis, Hydrographic patterns and vertical mixing in the equatorial Pacific along 150°W, *J. Geophys. Res.*, *97*, 611-626, 1992.

Carr, M.-E., M. R. Lewis, and D. Kelley, A physical estimate of new production in the equatorial Pacific along 150°W, *Limnol. Oceanogr.*, *40*, 138-147, 1995.

Chai, F., S. T. Lindley, and R. T. Barber, Origin and maintenance ,of a high nitrate condition in the equatorial Pacific, *Deep Sea Res., Part II*, *43*, 1031-1064, 1996.

Chavez, F. P., and R. T. Barber, An estimate of new production in the equatorial Pacific, *Deep Sea Res., Part A*, *34*, 1229-1243, 1987.

Chavez, F. P., S. K. Service, and S. E. Buttrey, Temperature-nitrate relationships in the central and eastern equatorial Pacific, *J. Geophys. Res.*, *101*, 20,553-20,563, 1996.

Dandonneau, Y., Monitoring the sea surface chlorophyll concentration in the tropical Pacific: Consequences of the 1982-83 El Niño, *Fish. Bull.*, *84*, 687-695, 1986.

Dandonneau, Y., Surface chlorophyll concentration in the Tropical Pacific Ocean: An analysis of data collected by merchant ships from 1978 to 1989, *J. Geophys. Res.*, *97*, 3581-3591, 1992.

Dandonneau, Y., Sea-surface partial pressure of carbon dioxide in the eastern equatorial Pacific (August 1991 to October 1992): A multivariate analysis of physical and biological factors, *Deep Sea Res., Part II*, *42*, 349-364, 1995.

Dandonneau, Y., and G. Eldin, Southwestward extent of chlorophyll-enriched waters from the Peruvian and equatorial upwellings between Tahiti and Panama, *Mar. Ecol. Prog. Ser.*, *38*, 283-294, 1987.

Delcroix, T., and J. Picaut, Zonal displacement of western equatorial Pacific fresh pool, *J. Geophys. Res.*, *103*, 1087-1098, 1998.

Dequé, M., C. Dreverton, A. Braun, and D. Cariolle, The ARPEGE/IFS atmosphere model: a contribution to the French community climate modelling, *Clim. Dyn.*, *10*, 249-266, 1994.

Dugdale, R. C., and J. J. Goering, uptake of new and regenerated forms of nitrogen in primary productivity, *Limnol. Oceanogr.*, *12*, 196-206, 1967.

Eldin, G., Eastward flows of the south equatorial central Pacific, *J. Phys. Oceanogr.*, *13*, 1461-1467, 1983.

Eldin, G., M. Rodier, and M.-H. Radenac, Physical and nutrient variability in the upper equatorial Pacific associated with westerly wind forcing and wave activity, *Deep Sea Res., Part II*, *44*, 1783-1800, 1997.

Feely, R. A., R. Wanninkhof, C. E. Cosca, P. P. Murphy, M. F. Lamb, and M. D. Steckley, CO_2 distributions in the equatorial Pacific during the 1991-1992 ENSO event, *Deep Sea Res., Part II*, *42*, 365-386, 1995.

Firing, E., R. Lukas, J. Sadler, and K. Wyrtki, Equatorial undercurrent disappears during 1982-83 El Niño, *Science*, *222*, 1121-1123, 1983.

Goddard, L., and N. E. Graham, El Niño in the 1990s, *J. Geophys. Res.*, *102*, 10,423-10,436, 1997.

Grima, N., A. Bentamy, P. Delecluse, K. Katsaros, C. Levy, and Y. Quilfen, Sensitivity study of an OGCM to satellite wind-stress forcing, *J. Geophys. Res.*, in press, 1998.

Hayes, S. P., L. J. Mangum, J. Picaut, A. Sumi, and K. Takeuchi, TOGA/TAO: A moored array for real-time measurements in the tropical Pacific Ocean, *Bull. Am. Meteorol. Soc.*, *72*, 339-347, 1991.

Herbland, A., A. Le Bouteiller, and P. Raimbault, Size structure of phytoplankton biomass in the equatorial Atlantic Ocean, *Deep Sea Res., Part A*, *32*, 819-836, 1985.

Honjo, S., Sedimentation of material in the Sargasso Sea at 5,367 m, *J. Mar. Res.*, *36*, 469-492, 1978.

Inoue, H. Y., M. Ishii, H. Matsueda, and M. Ahoyama, Changes in longitudinal distribution of the partial pressure of CO_2 (pCO_2) in the central and western equatorial Pacific, west of 160°W, *Geophys. Res. Lett.*, *23*, 1781-1784, 1996.

Kessler, W. S., and M. J. McPhaden, The 1991-1993 El Niño in the central Pacific, *Deep Sea Res., Part II*, *42*, 295-333, 1995.

Kessler, W. S., and B. A. Taft, Dynamic heights and zonal geostrophic transports in the central tropical Pacific during 1979-84, *J. Phys. Oceanogr.*, *17*, 97-122, 1987.

Kiefer, D. A., and B. G. Mitchell, A simple, steady state description of phytoplankton growth based on absorption cross section and quantum efficiency, *Limnol. Oceanogr.*, *28*, 770-776, 1983.

Ku, T., L. S. Luo, M. Kusakabe, and J. K. B. Bishop, ^{228}Ra derived nutrient budgets in the upper equatorial Pacific and the role of "new" silicate in limiting productivity, *Deep Sea Res., Part II*, *42*, 295-333, 1995.

Kuroda, Y., and M. J. McPhaden, Variability in the western equatorial Pacific Ocean during Japanese Pacific climate study cruises in 1989 and 1990, *J. Geophys. Res.*, *98*, 4747-4759, 1993.

Landry, M. R., et al., Iron and grazing constraints on primary production in the central equatorial Pacific: An EqPac synthesis, *Limnol. Oceanogr.*, *42*, 405-418, 1997.

Le Borgne, R., and M. Rodier, Net zooplankton and the biological pump: A comparison between the oligotrophic and mesotrophic equatorial Pacific, *Deep Sea Res., Part II*, *44*, 2003-2023, 1997.

Lehodey, P., M. Bertignac, J. Hampton, A. Lewis, and J. Picaut, El Niño-Southern Oscillation and tuna in the western Pacific, *Nature*, *389*, 715-718, 1997.

Lehodey, P., J.-M. André, M. Bertignac, J. Hampton, A. Stoens, C. Menkes, L. Mémery, and N. Grima, Predicting skipjack tuna forage distributions in the equatorial Pacific using a coupled dynamical bio-geochemical model, *Fish. Oceanogr.*, in press, 1998.

Levy, M., Modélisation des processus biogéochimiques en Méditerranée Nord-Occidentale: Cycle saisonnier et variabilité mésoéchelle, Ph.D. dissertation, 331 pp., Univ. de Paris VI, Paris, 1996.

Loukos, H., Simulation du cycle océanique du carbone dans l'Atlantique équatorial. Validation de l'année 1983 (FOCAL), Ph.D. dissertation, 207 pp., Univ. de Paris VI, Paris, 1995.

Lukas, R., and E. Lindstrom, The mixed layer of the western equatorial Pacific Ocean, *J. Geophys. Res.*, *96*, 3343-3357, 1991.

MacIsaac, J. J., and R. C. Dugdale, The kinetics of nitrate and ammonia uptake by natural populations of marine phytoplankton, *Deep Sea Res., Oceanogr. Abstr.*, *16*, 45-57, 1969.

Mackey, D. J., J. Parslow, H. W. Higgins, F. B. Griffiths, and J. E. O'Sullivan, Plankton productivity and biomass in the western equatorial Pacific: Biological and physical controls, *Deep Sea Res., Part II*, *42*, 499-533, 1995.

Maes, C., G. Madec, and P. Delecluse, Sensitivity of an equatorial Pacific OGCM to the lateral diffusion, *Mon. Wea. Rev.*, *125*, 958-971, 1997.

Martin, J. H., Glacial-interglacial CO_2 change: The iron hypothesis, *Paleoceanography*, *5*, 1-13, 1990.

McCarthy, J. J., C. Garside, J. L. Nevins, and R. T. Barber, New production along 140°W in the equatorial Pacific during and after the 1992 El Niño event, *Deep Sea Res., Part II*, *43*, 1065-1093, 1996.

McPhaden, M. J., TOGA-TAO and the 1991-93 El Niño-Southern Oscillation event, *Oceanography*, *6*, 36-44, 1993.

McPhaden, M. J., J. A. Proehl, and L. M. Rothstein, The interaction of equatorial Kelvin waves with realistically sheared zonal currents, *J. Phys. Oceanogr.*, *16*,1499-1515, 1986.

Menkes, C., J.-P. Boulanger, and A. J. Busalacchi, Evaluation of TOPEX and basin-wide Tropical Ocean and Global Atmosphere-Tropical Atmosphere Ocean sea surface topographies and derived geostrophic currents, *J. Geophys. Res.*, *100*, 25,087-25,099, 1995.

Morel, A., Light and marine photosynthesis: A spectral model with geochemical and climatological implications, *Prog. Oceanogr.*, *26*, 263-306, 1991.

Morel, A., and J.-F. Berthon, Surface pigments, algal biomass profiles, and potential production of the euphotic layer: Relationships reinvestigated in view of remote-sensing applications, *Limnol. Oceanogr.*, *34*, 1545-1562, 1989.

Moutin, T., and B. Coste, Campagne Océanographique OLIPAC à Bord du N. O. L'Atalante, 3 Novembre - 1er Décembre 1994; Recueil Des Données, *data report*, 266 pp., Cent. d'Océanol. de Marseille, France, 1996.

Murray, J. W., R. T. Barber, M. R. Roman, M. P. Bacon, and R. A. Feely, Physical and biological controls on carbon cycling in the equatorial Pacific, *Science*, *266*, 58-65, 1994.

Murray, J. W., E. Johnson, and C. Garside, A U.S. JGOFS process study in the equatorial Pacific (EqPac): Introduction, *Deep Sea Res., Part II*, *42*, 275-293, 1995.

Najjar, R. G., J. L. Sarmiento, and J. R. Toggweiler, Downward transport and fate of organic matter in the ocean: Simulation with a general circulation model, *Global Biogeochem. Cycles*, *6*, 45-76, 1992.

National Oceanic and Atmospheric Administration (NOAA), *Climate Diagnostics Bulletin*, Climate Analysis Center, Washington, D.C., 1994.

Oudot, C., and Y. Montel, A high sensitivity method for the determination of nanomolar concentrations of nitrate and nitrite in seawater with a Technicon AutoAnalyser II, *Mar. Chem.*, *24*, 239-252, 1988.

Peña, M. A., M. R. Lewis, and J. J. Cullen, New production in the warm waters of the tropical Pacific Ocean, *J. Geophys. Res.*, *99*, 14,255-14,268, 1994.

Philander, S. G., *El Niño, La Niña, and the Southern Oscillation*, 293 pp., Academic, San Diego, Calif., 1989.

Picaut, J., and T. Delcroix, Equatorial wave sequence associated with warm pool displacements during the 1986-1989 El Niño-La Niña, *J. Geophys. Res.*, *100*, 18,393-18,408, 1995.

Picaut, J., A. J. Busalacchi, M. J. McPhaden, L. Gourdeau, F. I. Gonzalez, and E. C. Hackert, Open-ocean validation of TOPEX/POSEIDON sea level in the western equatorial Pacific, *J. Geophys. Res.*, *100*, 25,109-25,127, 1995.

Picaut, J., M. Ioualalen, C. Menkes, T. Delcroix, and M. J. McPhaden, Mechanism of the zonal displacements of the Pacific warm pool: Implications for ENSO, *Science*, *274*, 1486-1489, 1996.

Price, N. M., B. A. Ahner, and F. M. M. Morel, The equatorial Pacific Ocean: Grazer-controlled phytoplankton populations in an iron-limited ecosystem, *Limnol. Oceanogr.*, *39*, 520-534, 1994.

Radenac, M.-H., and M. Rodier, Nitrate and chlorophyll distributions in relation to thermohaline and current structures in the western tropical Pacific during 1985-89, *Deep Sea Res., Part II*, *43*, 725-752, 1996.

Raimbault, P., G. Slawyck, B. Coste, and J. Fry, Feasibility of using an automated procedure for the determination of seawater nitrate in the 0-100 nM range: Examples from field and cultures, *Mar. Biol.*, *104*, 347-351, 1990.

Reynolds, R. W., and T. M. Smith, Improved global sea surface temperature analyses using optimum interpolation, *J. Climate*, *7*, 929-948, 1994.

Smolarkiewicz, K. P., and T. L. Clark, The multidimensional positive definite advection transport algorithm: Further developments and applications, *J. Comput. Phys.*, *67*, 396-438, 1986.

Stoens A., C. Menkes, Y. Dandonneau, and L. Mémery, New production in the equatorial Pacific: A coupled dynamical-biogeochemical model, *Fish. Oceanogr.*, in press, 1998.

Strickland, J. D. H., and T. Parsons, A practical handbook of seawater analysis, *Fish. Res. Board Can. Bull.*, *167*, 1-310, 1972.

Tans, P. P., I. Y. Fung, and T. Takahashi, Observational constraints on the global atmospheric CO_2 budget, *Science*, *247*, 1431-1438, 1990.

Thomas, C., Modélisation tridimensionnelle des champs de nitrate et d'oxygène et de la production nouvelle dans l'Océan Atlantique tropical en 1982-1984, Ph.D. dissertation, 194 pp., Univ. Paul Sabatier, Toulouse, France, 1995.

Thomas, W. H., Anomalous nutrient-chlorophyll interrelationships in the offshore eastern tropical Pacific Ocean, *J. Mar. Res.*, *37*, 327-335, 1979.

Toggweiler, J. R., and S. Carson, What are upwelling systems contributing to the ocean's carbon and nutrient budgets?, in *Upwelling in the Ocean: Modern Processes and Ancient Records*, edited by C. P. Summerhayes et al., pp. 337-360, John Wiley, New York, 1995.

Vialard, J., and P. Delecluse, An OGCM study for the TOGA decade, I, Role of salinity in the physics of the western Pacific fresh pool, *J. Phys Oceanogr.*, *28*, 1071-1088, 1998a.

Vialard, J., and P. Delecluse, An OGCM study for the TOGA decade, II, Barrier layer formation and variability, *J. Phys Oceanogr.*, 28, 1089-1106, 1998b.

Walsh, J. J., Herbivory as a factor in patterns of nutrient utilization in the sea, *Limnol. Oceanogr., 21*, 1-13, 1976.

Wong, C. S., Y.-H. Chan, J. S. Page, R. D. Bellegay, and K. G. Pettit, Trends of atmospheric CO_2 over Canadian WMO background stations at ocean weather station P, Sable Island, and Alert, *J. Geophys. Res., 89*, 9527-9539, 1984.

Wong, C. S., Y.-H. Chan, J. S. Page, G. E. Smith, and R. D. Bellegay, Changes in equatorial CO_2 flux and new production estimated from CO_2 and nutrient levels in Pacific surface waters during the 1986/87 El Niño, *Tellus, Ser. B, 45*, 64-79, 1993.

Wyrtki, K., An estimate of equatorial upwelling in the Pacific, *J. Phys. Oceanogr., 11*, 1205-1214, 1981.

Wyrtki, K., and B. Kilonsky, Mean water and current structure during the Hawaii-to-Tahiti shuttle experiment, *J. Phys. Oceanogr., 14*, 242-254, 1984.

Yentsch, C. S., and D. W. Menzel, A method for the determination of phytoplankton chlorophyll and phaeophytin by fluorescence, *Deep Sea Res., Oceanogr. Abstr., 10*, 221-231, 1963.

Yoder, J. A., C. R. McClain, G. C. Feldman, and W. E. Esaias, Annual cycles of phytoplankton chlorophyll concentrations in the global ocean: A satellite view, *Glob. Biogeochem. Cycles, 7*, 181-193, 1993.

J.-M. André and C. Navarette, Centre ORSTOM, BP A5, 98848 Nouméa Cédex, Nouvelle Calédonie, France.

Y. Dandonneau, N. Grima, L. Mémery, C. Menkès, M.-H. Radenac, and A. Stoens, LODYC, Univ. Pierre et Marie Curie, case 100, 4 place Jussieu, 75252 Paris Cédex 05, France. (e-mail: yd@lodyc.jussieu.fr, menkes@lodyc.jussieu.fr, mhr@lodyc.jussieu.fr, astlod@ipsl.jussieu.fr)

G. Eldin, Laboratoire d'Etudes en Géophysique et Océanographie Spatiales, 18 avenue Edouard Belin, 31401 Toulouse Cédex 4, France.

T. Moutin and P. Raimbault, Centre d'Océanologie de Marseille, Campus de Luminy, case postale 901, 13288 Marseille Cédex 09, France.

(Received September 8, 1997; revised August 10, 1998; accepted August 17, 1998.)

JOURNAL OF GEOPHYSICAL RESEARCH, VOL. 104, NO. C2, PAGES 3341–3356, FEBRUARY 15, 1999

Carbon and nitrogen uptake and export in the equatorial Pacific at 150°W: Evidence of an efficient regenerated production cycle

Patrick Raimbault, Gerd Slawyk, Benyahia Boudjellal,[1] Christine Coatanoan, Pascal Conan, Bernard Coste, Nicole Garcia, Thierry Moutin, and Mireille Pujo-Pay

Laboratoire d'Océanographie et de Biogéochimie (UMR CNRS 6535), Centre d'Océanologie de Marseille, Campus de Luminy, Marseille Cedex, France

Abstract. Biomass, inorganic carbon and nitrogen uptake, ammonium regeneration, nitrification, and vertical flux of particulate matter were measured in the equatorial Pacific at 21 daily productivity stations occupied on a meridional transect (150°W) between 1°N and 16°S. Three areas could be distinguished along the transect: (1) the equatorial area between 1°N and 6°S, where nitrate concentrations were typically eutrophic, reaching up to 3 μg-at L^{-1} in surface waters; (2) an intermediate mesotrophic area between 6° and 10°S, where surface nitrate concentrations decreased from 1 μg-at L^{-1} to zero; and (3) the oligotrophic area beyond 10°S, characterized by warm and nitrate poor waters. Although nitrate was the main form of inorganic nitrogen available for phytoplankton growth (70%–100% of total), its uptake was severely retarded in the equatorial sector. This lack of nitrate depletion in the equatorial sector between 0 and 6°S may in part result from the important ammonium supply (100 ng-at L^{-1} d^{-1}) which could sustain up to 85% of total inorganic nitrogen (nitrate + ammonium) utilization by phytoplankton. In addition, regenerated production also resulted from in situ nitrification (20–80 ng-atN L^{-1} d^{-1}) which can fuel 20%–100% of the nitrate uptake. Sinking particles represented <10% of total carbon fixation and ~10%–50% of new production in terms of carbon and nitrogen. From these discrepancies it was suggested that (1) new production rates were overestimated because of the high level of nitrification that provided "regenerated nitrate" and (2) advection of dissolved organic carbon and nitrogen played an important role in export. The specific hydrodynamical circulation, a conveyor belt generated by upwelling at the equator and downwelling some degrees south, associated with biological in situ remineralization of ammonium and nitrate as well, appeared to be a very efficient system for recycling inorganic nitrogen in the euphotic layer and thus for supporting the high regenerated production levels. On the other hand, the high nitrate/silicate ratios (>1.5) observed in the upwelling waters seemed to indicate that silicate is not efficiently recycled in this specific circulation system because of its low regeneration rate as well as its sink via rapidly sedimenting diatoms cell walls; this may be also true for iron. This reinforces the idea of Si and/or Fe limitation which was put forward earlier to explain low new production levels in the equatorial Pacific.

1. Introduction

New production, defined as the fraction of primary production driven by the input of new nutrients (usually nitrate) into the euphotic zone [*Dugdale and Goering*, 1967], and export production, defined as the fraction of primary production exported as particles (carbon and nitrogen) [*Eppley and Peterson*, 1979], are important variables that characterize the efficiency of carbon and nitrogen cycling and particle export from the biological food web in the ocean. These fractions of photosynthetic production play a role in the transport of atmospheric carbon dioxide to the ocean interior, and their quantification is needed to estimate the ability of the ocean to act as a sink for carbon dioxide. New production, and consequently carbon export by biological processes, is enhanced in regions of the ocean where turbulent mixing or upwelling enrich surface water with nutrients. Because of persistent upwelling, the equatorial Pacific includes areas of high productivity that may contribute significantly to high new production and thus to the global flux of carbon. Using data on the vertical flux of nitrate into the photic zone, new production in terms of carbon, and the proportion of new to total production (f ratio) [*Eppley and Peterson*, 1979], *Chavez and Barber* [1987] estimated that the central and eastern Pacific contributed 18%–56% of global new production. Recent investigations using direct measurements of new production with the ^{15}N tracer [*Dugdale et al.*, 1992; *Peña et al.*, 1992b; *McCarthy et al.*, 1996] showed a lower contribution (5%–17%). The lack of agreement between the latter observation and the former estimation arises from the high f ratio (0.4) used by *Chavez and Barber* [1987]. Direct measurements led to lower values of f (0.1–0.3) [*Dugdale et al.*,

[1]Now at Institut des Sciences de la Mer et de l'Aménagement du Littoral, Staoueli, Algeria.

Paper number 1998JC900004.
0148-0227/99/1998JC900004$09.00

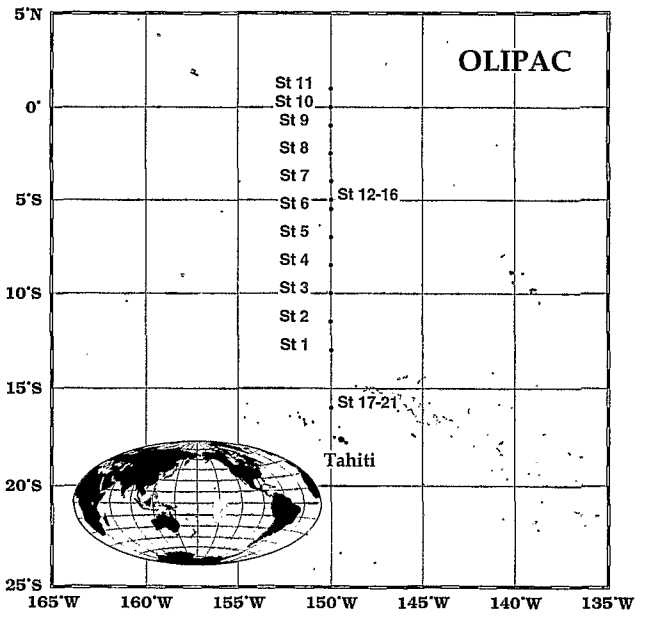

Figure 1. Study area with station locations.

1992; *McCarthy et al.*, 1996] indicating that although nitrate is the dominant form of inorganic nitrogen in the environment, most primary production is fueled by regenerated forms of nitrogen, namely, ammonium. In fact, nitrate supplied by equatorial upwelling is not immediately consumed but horizontally advected westward at ~40 cm s^{-1} and poleward according to the zonal current system driven at variable rates by easterly winds [*Kessler and McPhaden*, 1995]. Within 5° on either side of the equator, convergence results in downwelling and recirculation of the surface water back toward the equator. The freshly upwelled surface water at the equator would be expected to be enriched in macronutrients and micronutrients, and increased availability of light should allow the resident phytoplankton to take advantage of these nutrients. As this water is advected from the equator, it would be expected to mature with chlorophyll biomass increasing if there is a growth-grazing imbalance.

However, despite high macronutrient concentrations (nitrate 3 μg-at L^{-1}) [*Chavez and Barber*, 1987; *Murray et al.*, 1994] and an adequate input of solar radiation, phytoplankton pigment biomass is considerably lower than expected [*Thomas*, 1979]. The equatorial Pacific thus has been described as a high-nutrient/low-chlorophyll (HNLC) area [*Minas et al.*, 1986]. Several hypotheses have been evoked to explain this enigmatic feature, including physical processes [*Thomas*, 1972], initial nitrate concentration below some "physiological threshold" necessary to induce maximal uptake rates [*Wilkerson and Dugdale*, 1992], inhibition of nitrate uptake by ammonium [*Murray et al.*, 1989], grazing pressure which reduces biomass and in turn reduces absolute uptake rates [*Walsh*, 1974], and iron limitation [*Martin*, 1990]. As nitrate uptake is severely retarded, pCO_2 in surface waters remains elevated, and thus the sea surface becomes a net source of CO_2 to the atmosphere. Therefore the equatorial Pacific may be the largest marine source of CO_2 to the atmosphere [*Tans et al.*, 1990]. Despite its large area and the potential importance in the CO_2 exchange with the atmosphere through biological processes, there are relatively few data available on biological processes in the equatorial Pacific. Especially scarce are the direct measurements of new and regenerated production required for estimates of the f ratio as well as direct measurements of export production in the upper ocean in terms of sinking rates of particles. Prior to the present study the only detailed sections concerning new and regenerated production appear to be those of *Wilkerson and Dugdale* [1992] and of *McCarthy et al.* [1996]. However, measurements of inorganic nitrogen regeneration have not been done so far. Particle export using sediment traps has been mostly studied in deep waters. Corresponding measurements in the upper layer are sparse, although much of the particle cycle takes place in this layer. Although a positive correlation between surface primary productivity and the downward flux of particulate materials is well established in a qualitative sense [*Suess*, 1980; *Deuser et al.*, 1981], the quantitative nature of this relationship remains unclear.

The present investigation, conducted during the Oligotrophie en Pacifique (OLIPAC) cruise in November 1994, was undertaken as a part of the Joint Global Ocean Flux Study (JGOFS) program which is focused on the study of new and total production, the factors controlling these biological processes, and the export of photosynthesized materials to the deep ocean and sediments. This cruise provided the opportunity to measure directly inorganic carbon and nitrogen (nitrate and ammonium) uptake and ammonium regeneration using isotopic tracers (^{14}C and ^{15}N) as well as export production in terms of vertical particle flux using floating sediment traps on a meridional track along 150°W from 16°S to 1°N. This work also includes observations on nutrients and biomass (chlorophyll, carbon, and nitrogen).

2. Materials and Methods

This work was performed aboard the R/V *L'Atalante* during the OLIPAC cruise which formed a part of the JGOFS-France project. Hydrological measurements and biological experiments were conducted over the period November 3 to November 30 in the equatorial Pacific at 21 stations occupied along a transect at 150°W between 16°S and 1°N (Figure 1). Nutrients, particulate organic nitrogen (PON), particulate organic carbon (POC), chlorophyll a, ^{15}N and ^{14}C uptake rates, and sinking rates of carbon and nitrogen in particles were daily measured within the 0–200 m layer. The 1% light penetration depth (1% LPD) was calculated from a profile of photosynthetically active radiation (PAR) performed about noon using a biospheric instrument (PNF-300). Hydrographic measurements were done with a conductivity-temperature-oxygen-depth profiling system (CTOD Seabird, model SBE 911). Simultaneous in vivo chlorophyll fluorescence was measured by a SeaTech fluorometer (model SN 38S). Continuous multiparametric profiles obtained during the 0–200 m downcasts were examined to select 12 sampling depths for the upcasts in order to always encompass the chlorophyll a maximum. Samples were obtained with 12 L Niskin bottles with silicone rubber closures and tubing that had been carefully checked to avoid introducing toxic metals during sampling. Samples for nitrate + nitrite, silicate, and phosphate were collected in polyethylene flasks and were analyzed immediately after sampling on a Technicon Auto-Analyzer^{R} according to *Tréguer and LeCorre* [1975]. Samples for POC (3 L), PON (250 mL), and chlorophyll a (250 mL) were filtered using precombusted GF/F glass-fiber filters. Chlorophyll a concentration was determined by fluorimetry using

the methanol extraction procedure as described by *Raimbault et al.* [1988]. The filters for POC were kept dry until later analysis in the lab with a carbon-hydrogen-nitrogen (CHN) LECO 800 elemental analyzer. The filters were not treated to remove carbonates. Filters for PON were immediately treated on board using a persulfate wet-oxidation method [*Pujo-Pay and Raimbault*, 1994]. For dissolved organic nitrogen (DON), unfiltered samples were collected in 50 mL Pyrex bottles. Total nitrogen (TN = inorganic + particulate and dissolved organic nitrogen) were measured on board by the wet-oxidation procedure using the same reagent as for PON. DON concentrations were calculated as TN minus dissolved inorganic nitrogen (DIN) and PON.

For productivity measurements, samples collected before sunrise with Niskin bottles were poured into acid-cleaned polycarbonate (PC) bottles (1.2 or 2.4 L for ^{15}N experiments and 250 mL for ^{14}C experiments). The bottles were rinsed after use with 10% HCl, then with distilled water from a Milli Q ion exchange unit. Ambient nitrate, nitrite, and ammonium were immediately measured by directly pumping with the Technicon^R AutoAnalyser in the incubation bottles. Ammonium concentrations were determined according to *Tréguer and Le Corre* [1975] with a lower detection limit of 100 ng-at L^{-1}. Nitrate and nitrite concentrations in the nanomolar range (lower detection limit = 3 ng-at L^{-1}) were obtained from a sensitive method according to *Raimbault et al.* [1990]. Nitrogen 15–tracer additions as $K^{15}NO_3$ and $^{15}NH_4Cl$ (99 at.% ^{15}N) were usually 10%–20% of the ambient concentration. However, in nutrient impoverished oligotrophic waters, minimal additions of ^{15}N (42 ng-at L^{-1}) resulted in substrate enrichments of 50%–100%. It should be noted that these ^{15}N additions above tracer amount could significantly alter the nitrogen environment of phytoplankton and thus the measured uptake rates [*Allen et al.*, 1996; *Harrison et al.*, 1996]. The initial nitrate, nitrite, and ammonium concentrations were always verified after the tracer addition (T_0 concentrations). The PC bottles were then incubated under in situ conditions. The in situ array was typically launched at dawn and recovered after sunset (i.e., 12 hours incubation period) during the first 11 stations along the transect. During two repeating stations at 5° and 16°S incubation lasted 24 hours. Following incubation, concentrations of DIN were again measured directly in the PC flasks. The samples were then filtered onto 25 mm precombusted GF/F filters using low vacuum (<100 mm Hg). Subsequent to filtration, the filters were dried at 60°C and stored with dessicant. A 300 mL GF/F filtrate was again filtered on a 0.2 μm Anopore membrane and directly collected in a 500 mL Pyrex bottle (Duran Schott). These <0.2 μm filtrates were poisoned with $HgCl_2$ (20 μg mL^{-1}) and kept in the dark at ambient temperature until laboratory processing to determine ^{15}N enrichment in the DIN and DON pool according to the method described by *Slawyk and Raimbault* [1995]. In this procedure all DIN and DON forms were removed from the filtrate as ammonium sulfate by successive diffusion and collection on glass-fiber filters appropriate for the mass spectrometric assay. The first diffusion step allowed to obtain the final ^{15}N enrichment of the DIN pool and thus to estimate isotope dilution of the tracer. The second diffusion following a wet oxidation of DON was done to estimate the ^{15}N abundance in the DON pool. This procedure was improved to estimate nitrification (oxidation of ammonium to nitrate) by measuring the ^{15}N enrichment in the nitrate pool from some filtrates of ammonium uptake experiments. To do this, Devarda alloy was added (300 mg) to reduce nitrate to ammonium after the initial ^{15}N-labeled ammonium had been removed (first diffusion step). The liberated ammonium derived from the reduction step was then trapped on a filter by a further diffusion step. All filters containing particles and trapped ammonium were analyzed for ^{15}N content using a continuous-flow method (Europa Scientific in which Dumas combustion (Roboprep-CN) is linked on-line to a triple collector mass spectrometer (tracer-mass) via a capillary interface based on the design of *Preston and Owens* [1983]. Mass-spectrometric signals were used to calculate ^{15}N abundance in PON, DIN, and DON. Total beam (mass 28, 29, and 30) intensities were used to estimate PON (μg-at L^{-1}). The transport rate of nitrogen from the DIN pool to the PON pool; that is, the net DIN uptake rate (ρDIN, in ng-at L^{-1} h^{-1}) was computed from an equation based on a value for final PON concentration [*Dugdale and Wilkerson*, 1986]:

$$\rho\mathrm{DIN} = [(R_{\mathrm{PON}}/R_{\mathrm{DIN}})T][\mathrm{PON}] \quad (1)$$

where R_{PON} and R_{DIN} are the ^{15}N atom percent excess enrichment in the PON and DIN pool, respectively. [PON] corresponds to the final PON concentration. T is the incubation period in hours. Ammonium regeneration was estimated using the initial and final ^{15}N-NH_4 enrichment according to *Glibert et al.* [1982]. Ammonium uptake rates were corrected for isotopic dilution by using for R_{DIN} in (1) the mean value between initial and final enrichment in the ammonium pool ($\bar{R}_{\mathrm{NH_4}}$). No significant isotope dilution was detected for nitrate, so that R_{DIN} for nitrate in (1) corresponds to the initial ^{15}N atom percent excess enrichment in the nitrate pool ($R_{\mathrm{NO_3}}$). Nitrification rates (ρnit, in ng-at L^{-1} h^{-1}) were calculated as follows:

$$\rho\mathrm{nit} = [(R_{\mathrm{NO_3}}/R_{\mathrm{NH_4}})T][\mathrm{NO_3}] \quad (2)$$

where $R_{\mathrm{NO_3}}$ and $[\mathrm{NO_3}]$ are the ^{15}N atom percent excess enrichment and the final concentration (initial + carrier addition) of nitrate measured by mass spectrometry. $\bar{R}_{\mathrm{NH_4}}$ is the mean ^{15}N enrichment of ammonium.

The f ratio was calculated from

$$f = \rho\mathrm{NO_3}/(\rho\mathrm{NO_3} + \rho\mathrm{NH_4}) \quad (3)$$

No corrections were made for the possible contribution of urea since urea uptake was not measured.

Carbon fixation was measured in four 250 mL aliquots collected in PC bottles and incubated at the same depth and during the same time interval as for the ^{15}N uptake experiments. Each incubation bottle was spiked with 20 μCi of $NaH^{14}CO_3$ to initiate incubation. An extra sample was inoculated with ^{14}C and immediately filtered to determine abiotic fixation. After incubation, samples were filtered onto Whatman GF/F filters at <100 mm Hg, and the filters were placed in scintillation vials. To chase inorganic ^{14}C on the filters, 250 μL of HCl 0.5 N were added, and after 6–12 hours the filters were counted in 10 mL Aquasol in a liquid scintillation counter. All fixation rates were corrected for dark fixation determined at each depth using a dark bottle incubated under the same conditions as light bottles.

Some ^{15}N and ^{14}C samples were filtered on 0.2 μm Anopore membranes. While Anopore 0.2 μm membranes retained much more particulate nitrogen (up to 40% in low-PON waters) than GF/F filters (Figure 2a), the ^{15}N uptake rates obtained from these former membranes compared quite well with those obtained from GF/F filters (Figure 2b), indicating that

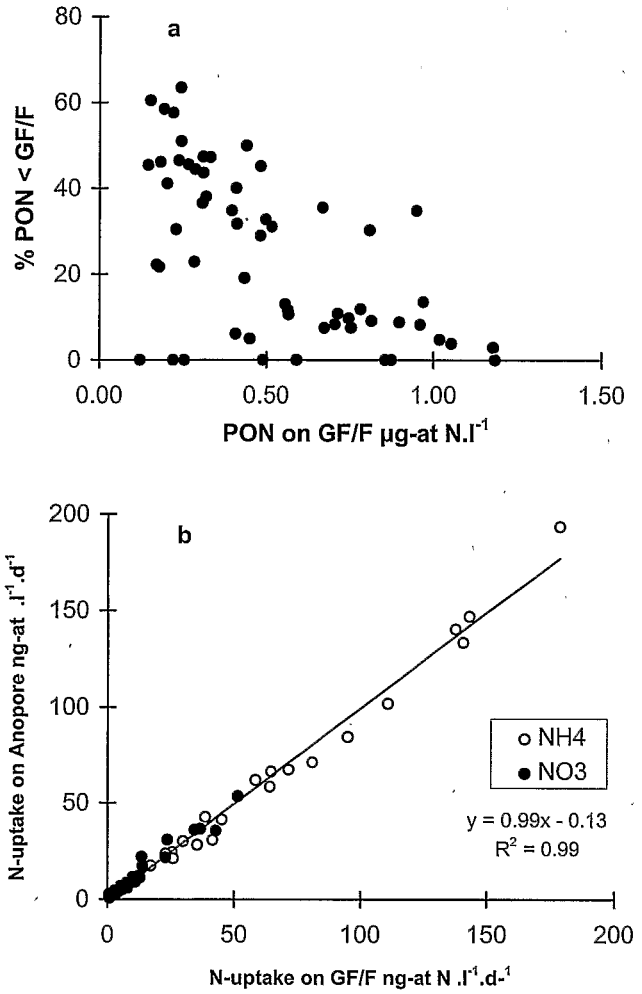

Figure 2. (a) Percentage of particulate organic nitrogen (PON) passing through GF/F filters and retained by 0.2 μm Anopore membranes (%PON < GF/F) versus PON retained by GF/F filters. (b) Efficiency of the GF/F filters compared to 0.2 μm Anopore membranes to measure inorganic nitrogen uptake.

glass-fiber filters were fully adequate for ^{15}N uptake measurements. Ten identical comparisons performed with the ^{14}C tracer gave similar results with no significant underestimation of primary production rates when using GF/F filters instead of Anopore 0.2 μm membranes (C uptake on GF/F = 95.4 ± 16% ^{14}C uptake on Anopore). Downward fluxes of particulate matter (PM) were measured in free-floating sediment traps (PPS4) deployed at a depth of 200 m. These cylindrical sediment traps have a mouth area of 0.05 m^2 and a height of 1.20 m. In our system the trap material was concentrated in a polyvinyl receptacle (10 cm height) placed at the bottom of the trap. The flasks were isolated from further inputs during launching and recovery by a valve that was activated by an electronic device with a timer. The collected flask was filled with filtered seawater containing no preservatives. In order to avoid microbial degradation of the PM to a maximum, traps were deployed during short time intervals (10 hours along the transect and 22 hours at 5° and 16°S) in parallel with the in situ ^{14}C and ^{15}N incubations. Estimates of the total particle flux were made gravimetrically. PM was filtered onto tared 25 mm precombusted GF/F filters immediately after recovery. Swimmers were scarce but when present were immediately removed from the filter using forceps. To eliminate residual salt water, filters were given three brief rinses with deionized water. They were then dried at 60°C and placed in a dessicator with silica gel and stored dry until they could be reweighed at the laboratory. After weighing, filters were analyzed with a CHN LECO 800 to determine the carbon and nitrogen content of the PM.

To facilitate comparisons with data from literature, all sediment fluxes as well as production rates were converted in daily rates. For heterotrophic processes (ammonium regeneration and nitrification) and sediment flux we assume no significant influence of the photoperiod; hourly rates were therefore multiplied by 24. For ammonium and nitrate uptake, some direct comparisons between 12 and 24 hour incubations were performed. During the transect, where in situ incubations were stopped at sunset, some subsamples were placed in a deck incubator for the night period before filtration (24 hours for total incubation). While nitrate was not taken up during the night period (Figure 3a), a significant ammonium uptake occurred (Figure 3b). According to these results, ammonium uptake rates obtained from 12 hour incubations (stations 1–11) were multiplied by a factor of 1.3 to compute daily rates. For ^{14}C fixation, such comparative experiments have not been performed, and we assume that dark fixation of carbon did not occur. As for nitrate experiments, the daily rates were estimated from 12 hour rates.

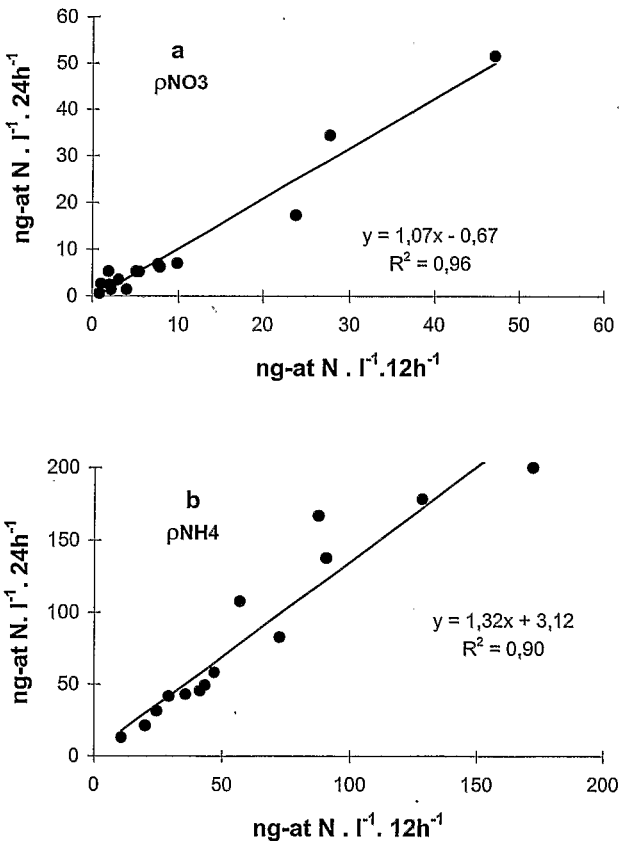

Figure 3. Comparison between 24 hour light-dark and 12 hour light incubations from nitrate and ammonium uptake experiments.

3. Results

3.1. Hydrography, Nutrient, and Biomass Distribution

Data shown throughout the paper are limited to the 0–200 m water column. The south-north distributions of temperature, salinity, nutrients, biomass in terms of chlorophyll, POC, and PON are shown in Figures 4 and 5. Surface temperatures (Table 1) were similar to those observed in February 1988 during the WEC88 cruise [*Carr et al.*, 1992] and in February 1992 during the first Eqpac survey (JGOFS TT07) by *Murray et al.* [1995], but they were a little higher than those noted by *Murray et al.* [1995] in September 1992 (JGOFS-TTO11 cruise), during the typical upwelling season, when surface temperature never reached 28°C and were <25°C at the equator. The contour plot of temperature (Figure 4a) revealed that warm water (>27°C) was always present between surface and ~100 m depth except at 16°S where this isotherm was located near 20 m. The isotherm 28°C surfaced at 16°S, slightly deepened until 100 m at the equator, and again reached the surface at 1°N. Typical upward doming and spreading of isotherms were absent at the equator; this was also observed by *Murray et al.* [1995] in February 1992 during the El Niño event. However, the depth of the mixed layer increased drastically toward the equator from ~40 to 130 m (Table 1). The salinity distribution (Figure 4b) depicted the typical feature with low surface values at the equator (<35.3 practical salinity unit (psu)). The salinity front, generally marked by the outcrop of the 35 psu isohaline at surface near the equator separating northern low-salinity water from southern high-salinity water [*Murray et al.*, 1995; *Carr et al.*, 1992], was not clearly visualized here. The isohaline 35 psu was found at depths >300 m in the southern part of the transect and at ~180 m at the equator. A salinity front was visible between 11° and 12°S where low-salinity water met high-salinity subtropical water. Dense water subducted to form a characteristic high-salinity tongue (>36 psu) located in the upper thermocline between 100 and 200 m and then spreaded equatorward.

Nutrient distributions were generally comparable with those of *Wyrtki and Kilonsky* [1984]. In contrast to temperature, the deep nutrient isolines sunk from north to south; surface nutrients tended to be asymmetrically distributed with high surface values between 1°N and 6°S. The lowest concentrations were found in the mixed layer south of 10°S. The 2 μg-at L^{-1} isoline for nitrate, found at a depth >120 m between 16° and 8°S, rapidly rose to surface at 6°S (Figure 4c). Surface values for nitrate near the equator were lower than those encountered in April 1988 by *Peña et al.* [1992a] at 135°W (>4 μg-at L^{-1}) and in February–March 1988 by *Carr et al.* [1992] at 150°W (>5 μg-at L^{-1}) but were similar to those observed in February 1992 by *Murray et al.* [1995] at 140°W. Nitrate concentrations decreased abruptly at 8°S (<0.5 μg-at L^{-1}) and became <0.1 μg-at L^{-1} between surface and 100 m depth beyond 10°S poleward. At ~7°–10°S, high-nitrate water lay over low-nutrient water as a consequence of downwelling of high-salinity nutrient poor subtropical water. It should be noted that except for this latitude, the vertical distribution of nitrate was relatively uniform throughout the photic zone, even at the equator. The general distribution of phosphate (Figure 4d) was similar to the one of nitrate with highest concentrations (>0.3 μg-at L^{-1}) between 1°N and 6°S. As for nitrate, surface concentrations decreased southward but remained always at significant levels, even at 16°S where they reached 0.15 μg-at L^{-1} between 0 and 100 m. These significant amounts of phosphate in the superficial layer of the subtropical region confirmed previous observations from *Murray et al.* [1995]. The silicate distribution showed the same general pattern as the one for nitrate and phosphate, although concentrations along the transect were less variable than those for nitrate and phosphate (Figure 4e). The equatorial zone was enriched with silicate where concentrations were >1.5 μg-at L^{-1} but never reached 2 μg-at L^{-1} as observed in JGOFS 1992 cruises [*Murray et al.*, 1995]. Surface values decreased to 1 μg-at L^{-1} between 2.5° and 8°S and then remained constant beyond 10°S. Silicate poor waters have been previously noted in March 1988 [*Peña et al.*, 1991]. In spite of the similar general pattern in the geographical distribution of these three important nutrients for new production, differences in concentration changes between them (when moving in the South Pole direction) led to modifications of the N/Si/P molar ratio along the transect (Table 1). The nitrate/phosphate ratio (integrated over 150 m) decreased from 9 to 5 between 1°N and 8°S and remained ~1.5–2 south of 10°S. The molar nitrate/silicate ratio was >1.5 between 1°N and 6°S and <0.7 in the south. In comparison to the Redfield ratio and to the phytoplankton requirement [*Fleming*, 1939], these values indicate a deficit in nitrate and silicate relative to phosphate near the equator (5°N–6°S) and a deficit in nitrate relative to silicate and phosphate in the southern part of the transect. Similar low levels of silicate occurred in 1988 [*Dugdale et al.*, 1992] as a result of a relatively shallow depth of the upwelling source water. It should be noted that nutrient samples from depth >300 m showed typical N/Si/P Redfield ratios (~1/1/16). DON concentrations ranged from 3 to 7 μg-at L^{-1}, with high concentrations generally in the surface water and lowest concentrations below 150 m (Figure 4). Lowest surface concentrations (<5.5 μg-at L^{-1}) were located between 13° and 16°S. A DON maximum (>6.5 μg-at L^{-1}) was found in the upper 100 m between 6° and 10°S, coincident with the sharp decrease in surface nitrate (Figure 6). In the convergence region (11°–13°S), where subtropical water subducted below low-salinity equatorial water (see Figure 4b), surface DON concentrations rapidly decreased from 7 to <5.5 μg-at L^{-1} depicting a sort of DON front.

Concentrations of regenerated nitrogen forms, such as nitrite and ammonium, showed a particular distribution pattern characterized by the presence of two subsurface maxima located south of the equator. Nitrite, a tracer of subtropical water [*Wyrtki and Kilonsky*, 1984] presented a maximum of up to 0.5 μg-at L^{-1} along the thermocline south of the equator (Figure 4g). The ammonium maximum (up to 1 μg-at L^{-1}), centered around 80–100 m, was shallower than the nitrite maximum (Figure 4h). Both maxima were just below the chlorophyll maximum (Figure 4d). These subsurface maxima have also been observed in 1992 at 140°W by *Murray et al.* [1995], while only a small patch of ammonium (0.3 μg-at L^{-1} between 40 and 90 m) was detected at 1°S [*Wilkerson and Dugdale*, 1992]. Concentrations of both regenerated forms were always low or undetectable in the 0–60 m layer except near the equator where they reached 0.20 and 0.10 μg-at L^{-1} for ammonium and nitrite. In the oligotrophic region (around 16°S), ammonium was undetectable all over the water column, while a very narrow nitrite maximum (>0.1 μg-at L^{-1}) was observed near 140 m depth.

Vertical distributions of biomass are shown in Figure 5 in terms of chlorophyll, PON, and POC. Surface chlorophyll concentrations (Figure 5a) increased along the transect from 0.06 at 16°S to 0.35 μg-at L^{-1} at 1°N and were well correlated with

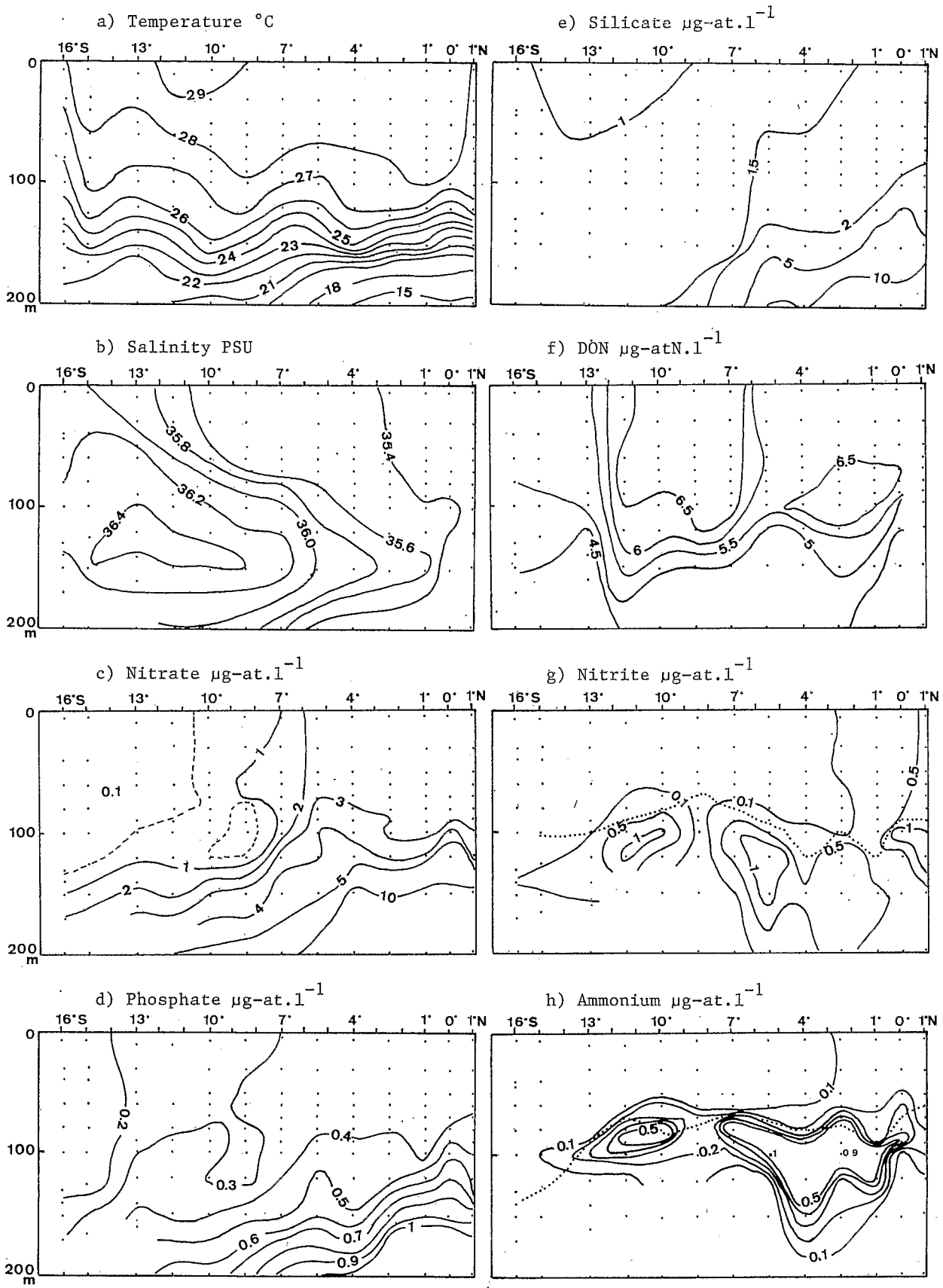

Figure 4. Contour plots of the 150°W transect, depth versus latitude: (a) temperature, (b) salinity, (c) nitrate, (d) phosphate, (e) silicate, (f) dissolved organic nitrogen (DON), (g) nitrite, and (h) ammonium. Dashed line on nitrite and ammonium panels represent depths of chlorophyll maximum and nitrite maximum, respectively. Dashed line on nitrate panel represents the 0.1 μg-at L^{-1} isoline.

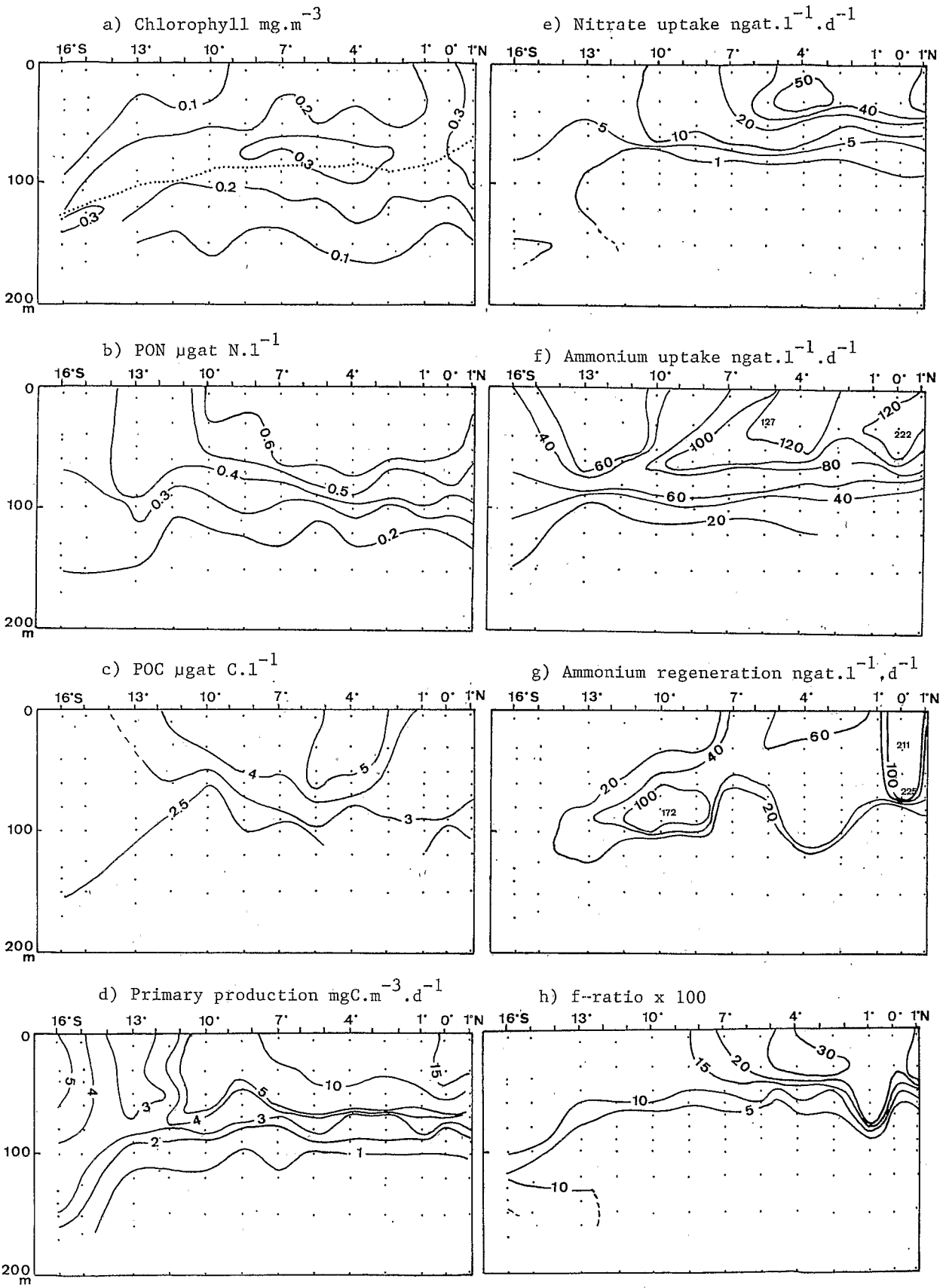

Figure 5. Contour plots of the 150°W transect, depth versus latitude: (a) biomass in terms of chlorophyll *a*, (b) particulate organic nitrogen (PON), (c) particulate organic carbon (POC), (d) primary production, (e) nitrate uptake, (f) ammonium uptake, (g) ammonium regeneration, and (h) *f* ratio (in percent). Dashed line on chlorophyll panel represents depth of 1% light penetration depth (LPD, lower limit of the euphotic zone).

Table 1. Sea Surface Temperature (SST), Mixed Layer Depth, and Integrated Values of Nitrate (Σ Nitrate), Chlorophyll *a* (Σ Chlorophyll), Nitrate/Silicate Ratio (NO_3/Si), Nitrate/Phosphate Ratio (NO_3/PO_4), and Particulate Nitrogen (ΣPON) and Carbon (ΣPOC) for the 1°N–16°S Transect Along 150°W

Station	Latitude °S	SST, °C	Mixed Layer, m	Σ Nitrate, mg-at m^{-2}	Σ Chlorophyll, mg m^{-2}	NO_3/Si	NO_3/PO_4	ΣPON, mg-at m^{-2}	ΣPOC, mg-at m^{-2}
					Equatorial				
11	−1	27.969	70	658.7	40.80	1.68	9.35	56.0	371.2
10	0	28.121	60	685.6	33.30	1.54	9.00	59.1	363.3
9	1	28.178	50	537.0	29.00	1.47	8.15	50.7	374.1
8	2.5	28.443	40	459.0	29.30	2.13	7.82	53.4	391.3
7	4	28.454	40	413.0	35.20	1.69	7.32	57.7	439.6
12	5	28.466	40	557.4	30.15	1.49	8.65	47.0	418.3
13	5.2	28.520	60	482.3	30.80		7.30		430.7
14	5.23	28.525	60	513.3	28.60		7.48	56.1	434.9
15	5.27	28.514	35	498.7	27.80		8.06		
16	5.33	28.550	45	499.9	31.31		7.47		357.0
6	5.5	28.397	20	510.0	30.10	2.01	8.58	57.5	437.3
					Mesotrophic				
5	7	28.764	30	279.7	25.80	1.42	6.01	58.2	352.8
4	8.5	29.006	40	116.6	25.60	0.70	2.70	46.2	347.8
3	10	29.185	20	98.2	23.70	0.56	2.38	49.1	333.7
					Oligotrophic				
2	11.5	29.063	30	91.2	21.80	0.61	2.14	42.1	424.2
1	13	28.817	10	84.4	25.13	0.49	2.00		
17	16	27.851	5	40.3	20.17		1.48	48.5	436.5
18	16	27.889	5	41.2	16.80		1.46	42.8	443.0
19	16	27.923	10	39.5	18.60				
20	16	28.122	10	36.0	19.90	0.26	1.49		
21	16	28.023	5	34.2	24.40				

The mixed layer depth was defined using the continuous profiles obtained with the conductivity-temperature-depth (CTD) probe to precisely determine the beginning of the thermocline (depth where temperature gradient was >0.1°C m^{-1}).

surface concentrations of nitrate ([chlorophyll] = 0.07 [nitrate] + 0.06; $r^2 = 0.80$; $n = 20$). All stations showed a typical subsurface chlorophyll maximum (SCM) where concentrations ranged from 0.2 to 0.3 μg L^{-1}, mostly at 70–80 m depth from 2° to almost 12°S and much deeper southward (140 m at 16°S). Within this SCM, concentrations were very homogeneous along the transect, only ranging from 0.27 to 0.33 μg L^{-1}. These levels were similar to those observed in the surface layer near the equator but were 2–6 times higher than surface values in the southern area. While the SCM was generally found just above the 1% LPD, the entire deep chlorophyll maximum (DCM) was below the euphotic zone at 16°S. Because of the relatively high deep chlorophyll concentrations in the subtropical region, the integrated values showed little geographical variation (Table 1). The areal chlorophyll content increased equatorward by a factor of 2 (from 20 to 35 mg m^{-2}) with a steep gradient around 1°S, while surface concentrations changed by a factor of 7. PON and POC concentrations showed little geographical variations (Figures 5b and 5c), and their depth profiles lacked pronounced subsurface maxima as observed for chlorophyll. Surface values were maximum near the equator with 0.65 and 4.5 μg-at L^{-1} for PON and POC, respectively. In the southern region, corresponding values were somewhat lower, 0.4 and 3.0 μg-at L^{-1} for PON and POC, respectively. These latter values, obtained from samples filtered on GF/F membranes, are close to those reported in 1988 by *Eppley et al.* [1992], *Peña et al.* [1991], and *Chavez et al.* [1996] for the same area. However, integrated values (0–150 m, Table 1) did not show obvious latitudinal variations as observed by *Eppley et al.* [1992], who integrated their values over the euphotic zone (1% LPD). Considering that chlorophyll *a* and particulate matter were present below this layer, the choice of the 1% LPD as the limit for their integrations might have led to underestimations of areal contents, especially in the southern oligotrophic region. The fact that POC and PON concentrations decreased slowly with depth in the southern region but changed rather rapidly with depth near the equator may add to this effect. In our case, integrations limited to the euphotic layer (down to the 1% LPD) would have resulted in areal contents of biomass and areal rates of primary productivity (see below) ~15%–20% lower than those obtained from integrations over the 0–150 m column. Moreover, the determination of PON using 0.2 μm Anopore membranes (Figure 2a) has confirmed the earlier observation that the use

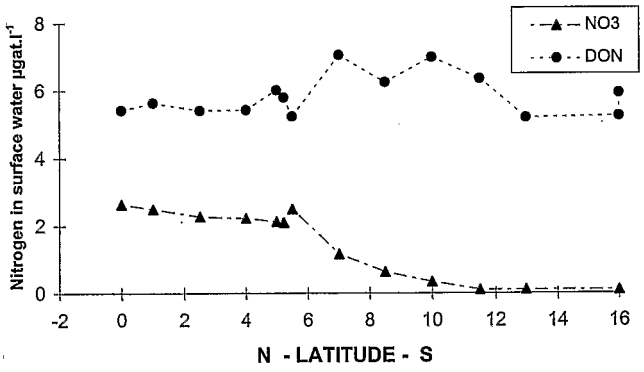

Figure 6. Latitudinal evolution along 150°W of surface concentrations of dissolved organic nitrogen (DON) and nitrate (NO_3).

Table 2. Depth of the Euphotic Zone (1% Light Penetration Depth (LPD)) and Integrated Values of Primary Production (ΣPP), New Production ($\Sigma\rho NO_3$), Regenerated Production ($\Sigma\rho NH_4$), f Ratio (Σ Ratio), and New Production in Terms of Carbon (Σ New Prod) Obtained by Multiplying Primary Production Rates by the Corresponding f Ratio for the 1°N–16°S Transect Along 150°W

Station	Latitude °S	1% LPD, m	ΣPP, mg C m^{-2} d^{-1}	$\Sigma\rho NO_3$, mg-at N m^{-2} d^{-1}	$\Sigma\rho NH_4$, mg-at N m^{-2} d^{-1}	Σf Ratio	Σ New Prod mg C m^{-2} d^{-1}
				Equatorial			
11	−1	65	990	1.65	9.7	0.145	143.92
10	0	77	1090	1.87	12.54	0.130	141.45
9	1	85	740	1.83	7.05	0.206	152.50
8	2.5	90	860	1.77	8.07	0.180	154.70
7	4	83	700	2.68	9.83	0.214	149.96
12	5	86		2.17	10.72	0.168	
13	5.2	87	610	2.05	8.94	0.187	113.79
14	5.23	88	880	2.27	10.42	0.179	157.42
15	5.27	85	870	2.05	8.94	0.187	
16	5.33	89	870				
6	5.5	nd	797	1.56	8.8	0.151	120.01
				Mesotrophic			
5	7	86		1.6	8.23	0.163	
4	8.5	87	620	0.9	7.54	0.107	66.11
3	10	90	570	1.62	6.94	0.189	107.87
				Oligotrophic			
2	11.5	98	370	0.47	4.38	0.097	35.86
1	13	103	290	0.488	5.5	0.081	23.63
17	16	127		1.58	8.23	0.161	
18	16	130		1.19	10.67	0.100	
19	16	125					
20	16	123	560	1.19	10.67	0.100	56.19
21	16	124	550	0.67	7.62	0.084	46.20

of GF/F filters leads to underestimates of the level of particulate matter [*Altabet*, 1990; *Slawyk and Raimbault*, 1995; *Pujo-Pay et al.*, 1997; *Libby and Wheeler*, 1997]. According to this latter observation, values of PON and POC given in this study as well as those from literature data have to be heightened by a factor of 1.5–2.

The distribution of hydrological and biological parameters clearly showed that the properties in terms of biomass varied much less than might be expected from nutrient distributions. However, on the basis of physical and chemical characteristics, three regions could be distinguished along the transect (Table 1). The first region is the oligotrophic region beyond 10°S, characterized by warm, high-salinity, and nitrate poor waters and a euphotic layer >100 m. In this region, areal contents were <100 μg-at m^{-2} and 25 mg m^{-2} for nitrate and chlorophyll, respectively. This area was also characterized by a low N/Si/P ratio, indicating a deficit in nitrogen with respect to the Redfield ratio. The second region is the equatorial region between 1°N and 6°S, where nitrate concentrations in surface waters were >2 μg-at L^{-1} and salinity was <35.5 PSU. Integrated values for nitrate and chlorophyll ranged from 400 to 700 mg-at m^{-2} and from 30 to 40 mg m^{-2}, respectively; the euphotic zone was <90 m thick. This region was characterized by a high NO_3/Si ratio, suggesting a deficit in silicate. The third region is the mesotrophic region between 6° and 10°S where surface nitrate rapidly decreased from 1 μg-at L^{-1} to undetectable values while integrated chlorophyll slightly decreased from 30 to 25 mg m^{-2}. This transitional area was also characterized by undetectable concentrations of ammonium at the surface (Figure 4h), high concentrations of DON, (6.5 μg-at L^{-1}, Figure 4f) in the 0–100 in layer, and decreasing NO_3/Si ratios (Table 1). The northern boundary of the oligotrophic zone was characterized by a salinity front and seemed to be the place of a convergence where surface water downwelled and forwarded to the equator at depths between 100 and 150 m.

3.2. Carbon Fixation and New and Regenerated Production

Primary production in terms of carbon strongly responded to nutrient enrichment of the euphotic zone. Fixation rates were >10 mg C m^{-3} d^{-1} (Figure 5d) in the equatorial zone where nitrate appeared close to the surface. Surface fixation rates ranged between 5 and 10 mg C m^{-3} d^{-1} in the mesotrophic region and were <4 mg C m^{-3} d^{-1} in the oligotrophic area, except at 16°S where five successive profiles gave a mean daily productivity of 5.13 ± 0.80 mg C m^{-3} d^{-1}. In this latter region, significant ^{14}C assimilation (>2 mg C m^{-3} d^{-1}) was measured far below the euphotic zone, until 140 m, while in the other sectors, photosynthetic activity stopped at ~1% LPD (~100 m). This deep primary production explained the small geographical changes in integrated production rates which ranged from 300–500 mg C m^{-2} d^{-1} in the south to 800–1000 mg C m^{-2} d^{-1} near the equator (Table 2). New (ρNO_3) and regenerated (ρNH_4) production rates were also highest in the surface nutrient-enriched area (Figures 5e and 5f). Nitrate uptake was more light-dependent than ammonium uptake, and rates were not significantly different from zero (<0.5 ng-at L^{-1} d^{-1}) below the euphotic zone, except at 13° and 16°S where ρNO_3 reached 4 ng-at L^{-1} d^{-1} in the DCM at 140 m depth. Regenerated production was significant below the 1% LPD (>40 ng-at L^{-1} d^{-1}) at all stations. Values for ρNH_4 were always higher than for ρNO_3 over the entire region, with maximal values occurring in the vicinity of the equator. However, at the equator, general high nutrient availability enhancement of ρNH_4 (by a factor of 3) was not as pronounced as enhancement

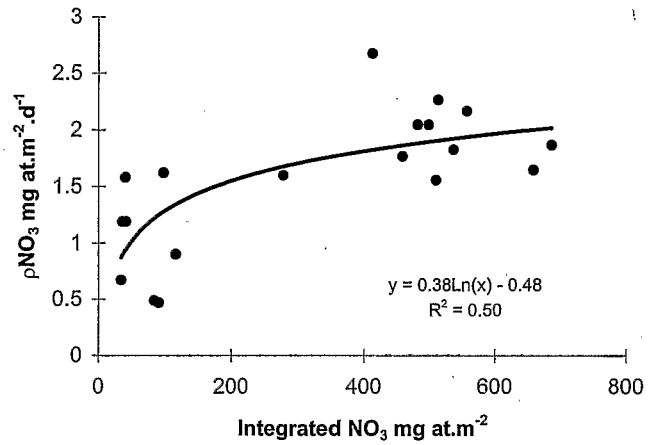

Figure 7. Relationship between the integrated nitrate concentration and the integrated nitrate uptake (ρNO_3) along the 150°W transect between 16°S and 1°N.

of ρNO_3 (by a factor 5). Integrated values of ρNH_4 showed no obvious latitudinal trend and could not be related to integrated values of ammonium concentration (Table 2). It should be remembered that ammonium uptake measured in the oligotrophic region could be overestimated because of the perturbation effect of the tracer addition. In contrast, a positive relationship was found between integrated ρNO_3 and nitrate concentration (Figure 7). Although integrated nitrate concentrations increased by a factor of 17 from the oligotrophic to the equatorial zone (Table 1), integrated new production rates increased only twofold to threefold (Table 2). In the equatorial region, ρNO_3 remained constant (2 mg-at m^{-2} d^{-1}) in spite of the significant increase of nitrate. Exterior to the equatorial zone, nitrate uptake was also poorly related to nitrate. The lack of a good relationship between nitrate concentration and ρNO_3 could explain the poor performance of models that use this relationship in the equatorial Pacific region.

3.3. Nitrogen Regeneration

Ammonium regeneration rates also showed important regional variations (Figure 5g). Regeneration was very active in surface waters around the equator with rates >100 ng-at L^{-1} d^{-1} and between 1° and 6°S with rates >60 ng-at L^{-1} d^{-1}. In the mesotrophic zone, surface values decreased down to 40 ng-at L^{-1} d^{-1}, but higher rates (>50 ng-at L^{-1} d^{-1}) were found at ~100 depth, associated with a subsurface maximum of ammonium. Ammonium regeneration was very low in surface waters of the oligotrophic zone (<20 ng-at L^{-1} d^{-1}) but showed an important subsurface maximum between 10° and 13°S associated with high ammonium concentrations (Figure 4g). At the most oligotrophic station (16°S), ammonium regeneration was low and more or less homogeneous over the water column (5–10 ng-at L^{-1} d^{-1}). Nitrification rates at the oligotrophic site were <5 ng-at L^{-1} d^{-1} in the surface layer but reached values >10 ng-at L^{-1} d^{-1} at depth (Figure 8). In the mesotrophic and upwelling area, nitrification rates reached 40 ng-at L^{-1} d^{-1}. The upwelling area was characterized by high nitrification rates in the whole upper layer, indicating that 20%–100% of nitrate uptake (new production) could be sustained by in situ nitrate regeneration.

3.4. The *f* Ratio

Figure 5h shows the distribution of the *f* ratio, calculated from daily rates of new production and regenerated production which were both corrected for isotope dilution (see section 2). There is a general decrease in *f* with depth due to the greater dependence of nitrate uptake on irradiance than on ammonium uptake. The geographical variation of the ratio is closely related to the distribution of nitrate concentration and nitrate uptake. Values of *f* increased from 16°S (<0.10) to the equatorial region (>0.30) but always rapidly decreased with depth. Values were generally <0.02 below 80 m except at 13° and 16°S where high nitrate uptake rates found in the DCM (below the 1% LPD) led to a ratio >0.15 at a depth >100 m. Values of integrated new and regenerated production as well as of *f* ratios given in Table 2 are consistent with the physical and chemical features of the three areas previously defined. The highest uptake rates were found in the equatorial region where *f* ranged from 0.15 to 0.21. In the mesotrophic region, uptake rates were somewhat lower, and *f* ranged from 0.11 to 0.19. The integrated *f* ratio was used to calculate new production from ^{14}C fixation rates (Table 2). New production appeared to be elevated in the equatorial zone (142 ± 16 mg C m^{-2} d^{-1}), was lower in the mesotrophic region (90 ± 29 mg C m^{-2} d^{-1}),

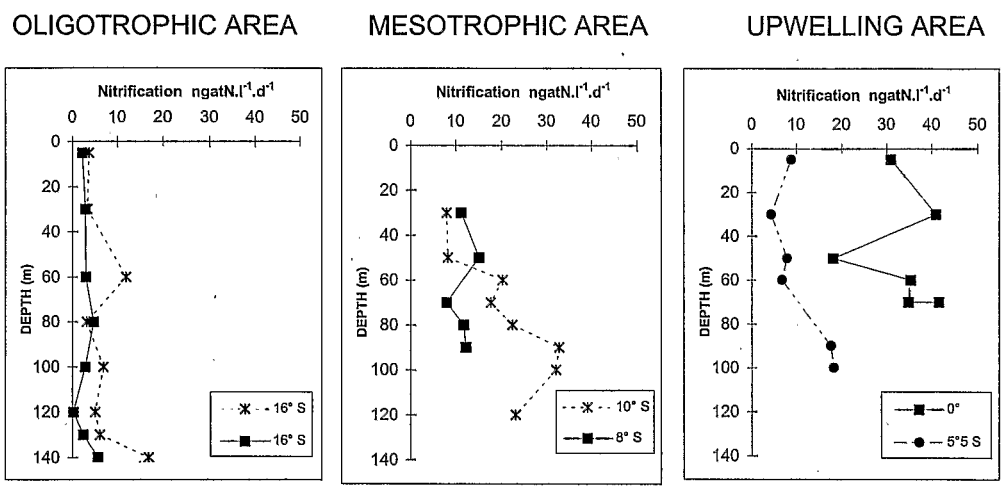

Figure 8. Profiles of ammonium oxidation (nitrification in ng-at L^{-1} d^{-1}) versus depth obtained from the three distinguished regions (see text).

and was lowest in the oligotrophic zone (40.5 ± 14 mg C m^{-2} d^{-1}). Mean total carbon fixation was compared with mean total nitrogen production ($\rho NO_3 + \rho NH_4$) in terms of atomic ρ_C/ρ_N ratio (Figure 9). Values of ρ_C/ρ_N ratios for the equatorial and mesotrophic zones (4 to 7.7 and 5.5, respectively) were close to the Redfield ratio. In the oligotrophic zone the ρ_C/ρ_N ratio was <5. This low ratio may be partly explained by an overestimation of nitrogen uptake in the upper nutrient-depleted layer, where ^{15}N tracer additions, even at nanomolar levels, might have led to an artificial increase in uptake rates. In contrast, the mean C/N composition ratio in seston along the transect was 7.8 ± 1.33 and agreed well with the Redfield ratio.

3.5. Export of Particulate Matter

Fluxes of PM, POC, and PON obtained from experiments with sediment traps are given in Figure 10. All fluxes depicted major latitudinal variations. Maximal fluxes were found in the equatorial region until 4°S, followed by a regular decrease until 10°S. Fluxes in the southern area were very low and showed no significant geographical trend. Spatial patterns in vertical fluxes of POC and PON were similar to those observed for total mass fluxes (PM). The C/N atomic ratio of the flux material was always higher than in the suspended material (Figure 9), increasing from 8–10 in the equatorial region to 10–14 in the oligotrophic area. This latter pattern suggests that marked losses in N occurred in the particles, while comparatively large amounts of C remained associated with particles. This is consistent with the finding that nitrogen is lost more rapidly than carbon from sinking particles [*Knauer et al.*, 1979; *Lohrenz et al.*, 1992]. To provide information on the proportion of total primary production leaving the euphotic zone in the form of sinking particles, we calculated export ratios of carbon (e_{POC} = POC_{flux}/PP) and nitrogen (e_{PON} = PON_{flux}/N uptake) according to *Murray et al.* [1989]. Both e_{POC} and e_{PON} varied along the transect (Figure 11) with the highest values occurring in the equatorial region, thus indicating a positive relationship between export, total primary production, and nitrate availability. Between 16° and 6°S both e_{POC} and e_{PON} values were very low and similar, indicating that only 1%–3% of nitrogen and carbon assimilated by phytoplankton left the euphotic zone in the form of sinking particles. In the equatorial region, rates of export increased to 8%–10% for carbon but only to 6%–8% for nitrogen, suggesting a different fate for carbon and nitrogen.

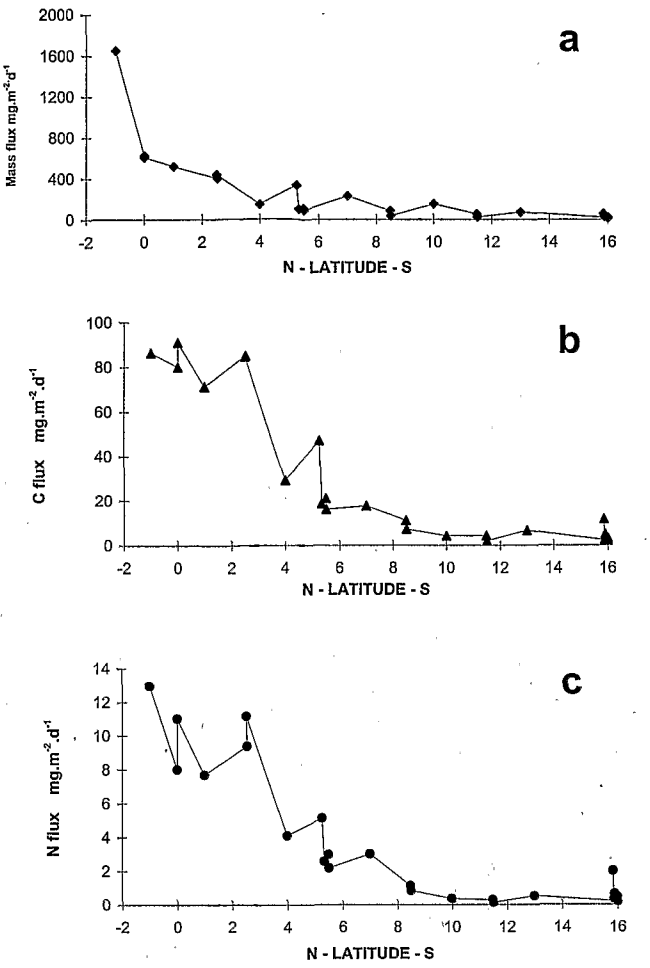

Figure 10. Latitudinal variation of downward flux of (a) particulate matter (mass flux), (b) particulate organic carbon (carbon flux), and (c) particulate organic nitrogen (nitrogen flux). Results from three repetitive stations conducted at 16°S are given.

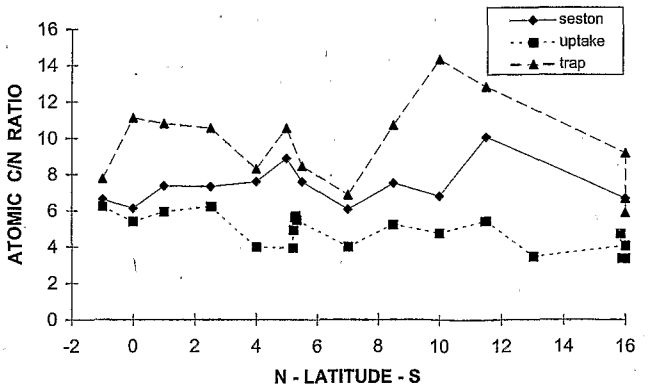

Figure 9. Latitudinal variation of the atomic C/N ratio in suspended materials (seston), trap-collected materials (trap), and from the ^{14}C and ^{15}N uptake experiments (uptake). All ratios are from integrated (0–150 m) values. Results from three repeating stations conducted at 16°S are given.

3.6. Discussion

3.6.1. New versus export production: Impact of DOM in improving C and N budgets. The period from 1991 to 1994 corresponded to a long-lived warm anomaly in the equatorial

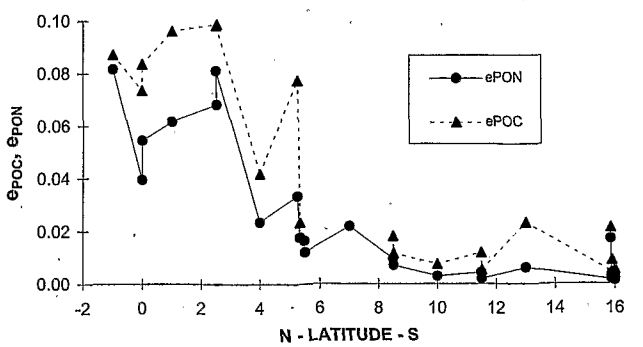

Figure 11. Latitudinal variation of the export ratio in terms of carbon (e_{POC}) and nitrogen (e_{PON}).

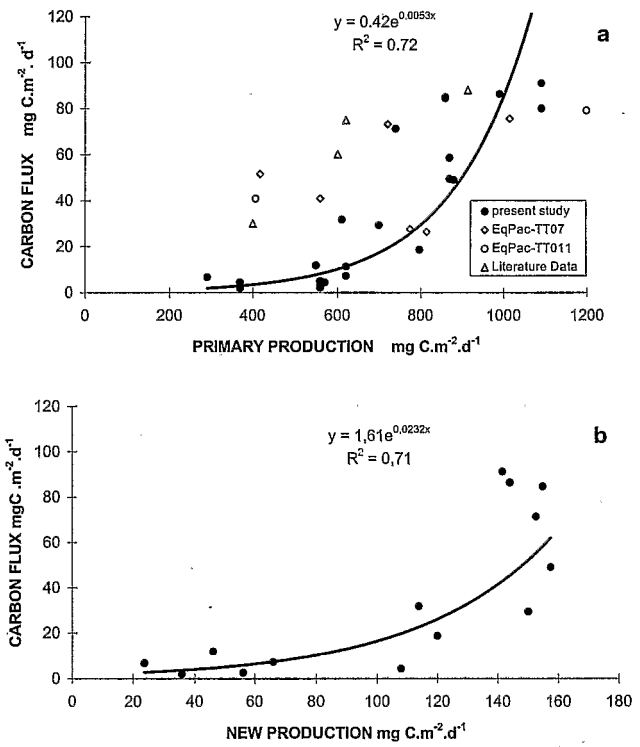

Figure 12. Plot of carbon flux (a) versus primary production and (b) versus new production calculated by multiplying primary production by the f ratio. TT011 and TT007 data are from *Murray et al.* [1996]. Others literature data are from *Chavez et al.* [1996], *Buesseler et al.* [1995], *Betzer et al.* [1984], and *Luo et al.* [1995]. The exponential relationships are calculated from data of this study (solid symbols).

Pacific with two El Niño events in 1991–1992 [*Kessler and McPhaden*, 1995]. Hydrological conditions prevailing during November 1994 were quite similar to those observed in spring 1992 by *Murray et al.* [1995] and typical of a moderate El Niño event, with surface temperatures 2°C higher than the annual mean and nitrate surface concentrations about half of average values [*Chavez et al.*, 1996]. In spite of these warm conditions, primary production (total and new production) in terms of carbon were as high as those observed during normal upwelling conditions. Mean values for total carbon fixation at the equator (950 mg C m^{-2} d^{-1}) were ~2 times higher than values from southern oligotrophic waters (440 mg C m^{-2} d^{-1}) beyond 10°S. These production rates are close to those observed at 135°W in the equatorial zone (1°N–1°S) as well as in the southern oligotrophic region (14°S) during March 1988, 1005 and 456 mg C m^{-2} d^{-1} respectively [*Peña et al.*, 1992], and to those found following the 1992 El Niño event during the EqPac cruises (1000–1500 mg C m^{-2} d^{-1} at the equator and 324–372 mg C m^{-2} d^{-1} at 12°S [*Barber et al.*, 1996]). New production rates near the equator (between 0 and 5°S) were ~140 mg C m^{-2} d^{-1} and were close to the value of 113 mg C m^{-2} d^{-1} found at 150°W during the WEC88 cruise [*Dugdale et al.*, 1992]. Our rates comprised those measured under El Niño (50 mg C m^{-2} d^{-1}) and non–El Niño (222 mg C m^{-2} d^{-1}) conditions [*McCarthy et al.*, 1996]. However, our nitrate uptake rates measured poleward to 5°S were much higher (by a factor of 2–3) than those found in 1988 by *Dugdale et al.* [1992]. In fact, in 1988 the area of high nitrate and ammonium uptake was limited to a narrow band near the equator, while during the present work, high productivity rates occurred far to the south (until 7°S).

There was a good agreement between new production (in terms of carbon) computed from direct measurements of nitrate uptake and the Redfield ratio ($\rho_{NO3} \times 6.6$) and new production obtained from ^{14}C fixation rates multiplied by the independently estimated f ratio. This seems to demonstrate that new production in terms of carbon in the equatorial Pacific may be estimated with confidence from measurements with the ^{15}N tracer and used for modeling purposes. Values of f found in this study (0.08–0.30) agree well with those noted by *Dugdale et al.* [1992] and *McCarthy et al.* [1996] but were much lower (twofold to fivefold) than those estimated from models of *Eppley and Peterson* [1979] and *Platt and Harrison* [1985]. This latter discrepancy seems to indicate that the equatorial upwelling, in spite of its nitrate rich waters, is distinct from coastal upwellings to which the latter f ratio models apply.

According to *Eppley and Peterson* [1979] the f ratio is defined as the fraction of total production (new production) that must leave the euphotic zone to balance the input of new inorganic nitrogen. However, our data show that the amount of carbon and nitrogen produced in the euphotic zone (new production) is always greater than the corresponding amount recovered in sediment traps. Export ratios (e_{POC} and e_{PON}, Figure 11) were significantly lower than f ratios, indicating that only a small part of new production is exported through sinking particles especially in the mesotrophic and oligotrophic area where export represented <10% of new production. However, we obtained a relationship between primary production and carbon flux at the base of the euphotic zone (Figure 12). Figure 12a, which includes data from literature, shows that our measurements of particulate carbon flux are comparable with direct measurements using other types of sediment traps and with indirect measurements using ^{234}Th [*Buesseler et al.*, 1995; *Murray et al.*, 1996] in areas where primary production is >600 mg C m^{-2} d^{-1}. For example, C and N particle fluxes measured at the equator (70–80 and 8–10 mg m^{-2} d^{-1}, respectively) are close to estimations of *Betzer et al.* [1984] obtained from sediment traps deployed at 900 m and to those of *Murray et al.* [1989] from the eastern Pacific. Along 140°W, *Buesseler et al.* [1995] and *Murray et al.* [1996] observed a particulate carbon export from the upper 100 m of ~25 mg C m^{-2} d^{-1} (at ~4°S) and an equatorial peak of 60 mg C m^{-2} d^{-1}, which are very close to our estimations. However, our sinking fluxes measured in less productive waters (<600 mg C m^{-2} d^{-1}) were much lower than those given for the same region by *Murray et al.* [1996], who placed their sediment traps at shallower depths (120 versus 200 m for ours). This difference between the collecting depth of the traps may explain the discrepancies between sinking rates since particle flux is highly dependent on sampling depth and decreases greatly between 100 and 200 m [*Luo et al.*, 1995]. On the other hand, our rates are consistent with those found in the oligotrophic Sargasso Sea [*Lohrenz et al.*, 1992]. Vertical carbon flux is exponentially related to new production (Figure 12b). This exponential model predicts that a threefold increase in new production, which occurs when moving from oligotrophic into equatorial waters, would result in a tenfold increase in the downward flux of organic material. The model also confirms differences in the fate of particulate organic matter; that is, particles are more strongly retained in the euphotic layer of unproductive oligotrophic areas than in the euphotic layer of productive upwelling areas [*Lohrenz et al.*, 1992].

Several reasons are evoked to explain the discrepancy between rates of new production measured with isotopic tracers and export production obtained from sediment traps. First, the discrepancy may be a result of a methodological bias since particles were collected 50 m below the euphotic zone. Second, the discrepancy may be caused by horizontal advection which explains the lack of agreement between new production and export measured at the same geographical location. The equatorial region is characterized by an active current system with the south equatorial current flowing to the west and the intense equatorial undercurrent flowing to the east. Therefore particulate materials produced in the upwelling area may be rapidly advected away and consequently would not fall strictly vertically.

Another possible cause of the discrepancy is that the f ratio used to calculate new production could be overestimated. Historically, regenerated production was measured exclusively using ammonium uptake. Dissolved organic nitrogen found in relatively high concentrations in marine waters, resulting from zooplankton excretion, bacterial remineralization, or direct release by phytoplankton cells, may represent a significant source of nitrogen for phytoplankton [*Antia et al.*, 1991; *Bronk et al.*, 1993]. More precise estimations of the f ratio would need measurements of DON uptake, especially urea. Inspecting data from literature, *Wafar et al.* [1995] have demonstrated that exclusion of urea uptake from the calculation overestimated the f ratio in upwelling and oceanic regions from 16% to 42%. Applying this correction to our data led to lower values for the f ratio in the equatorial (0.15) and the oligotrophic (<0.05) region. New production rates between 0 and 3°S calculated with these corrected values agreed rather well with sinking rates of particles, but discrepancies (up to 80%) between both rates still existed in the southern region. Failure to account for nitrification as a source of in situ regenerated nitrate could lead to a overestimation of the f ratio. As previously found by *Ward* [1985] and *Gentilhomme and Raimbault* [1994], nitrification rates found at the base of the euphotic zone were high enough to fuel the daily nitrate demand by phytoplankton. This led the latter authors to conclude that a great part of nitrate uptake was regenerated production rather than new production.

For many authors a further explanation for the disagreement between rates of new production and export production is that the horizontal advection or vertical mixing of dissolved organic matter (DOM) can exceed fluxes of sinking particles and thus appear as a major fate of new production [*Copin-Montégut and Avril*, 1993; *Peltzer and Hayward*, 1996]. *Toggweiler* [1989] reported that balance solely between upward nutrient flux and sinking particles in a three-dimensional modeling study led to overincreasing nutrient concentrations and particles fluxes. The most realistic simulations were obtained when half of the new production due to upwelled nutrient went into a pool of organic compounds. The release of DON in short-term incubation experiments has been reported for several types of marine waters [*Bronk et al.*, 1994; *Slawyk and Raimbault*, 1995]. Work on DI^{15}N losses performed during this cruise [*Slawyk et al.*, 1999] indicated that only a small fraction of $^{15}N\text{-}NO_3$ taken up (2%–10% in mesotrophic and oligotrophic regions) was ultimately found in the extracellular DON pool at the end of incubation. The percentage of nitrogen lost by phytoplankton as DON (DON release) was in fact higher than these values (by 1 order of magnitude) as a result of the dilution of the tracer nitrogen during incorporation in the initially unlabeled planktonic material [*Slawyk et al.*, 1999]. Consequently, the DON release via excretion, cell lysis, or sloppy feeding might represent at least ~20–100% of the new production. Moreover, the simultaneous decrease in nitrate and increase in DON (Figure 6), as surface water moves away from the equator, may be indicative of (1) net production of DON, (2) DON export as water moves poleward, and (3) DON accumulation in the convergence zone (Figure 4f). The meridional decrease in nitrate (from 2 to 0.24 = 1.76 μg-at L^{-1}) and increase of DON (from 5.7 to 6.9 = 1.20 μg-at L^{-1}) from the equatorial zone to the mesotrophic zone revealed that 68% of the nitrate that disappeared was accumulated as DON, a value close to the 81% estimate of *Libby and Wheeler* [1997]. Then we can hypothesize that a large fraction of inorganic nitrogen consumed in the equatorial zone is recovered in the dissolved organic pool in the mesotrophic area and transported meridionally away from the equator until 11°–13°S. Adding this DON production to the particulate matter flux would roughly balance the nitrogen budget in the euphotic zone. Similar data concerning DOC release are not yet available. However, from the likeness of the ρ_C/ρ_N and C/N ratios we may suggest that the ratio of release to export is the same for DOC and DON. This assumption is strengthened by the fact that a large increase of DOC in the upper layer occurred between 6° and 10°S [*Peltzer and Hayward*, 1996]. In this case, lateral advection of DOC would provide an important sink for assimilated carbon. One should emphasize that the DON accumulation as well as the high DOC content observed by *Peltzer and Hayward* [1996] occurred between 5° and 10°S, i.e., in the convergence zone. According to the three-dimensional circulation model of *Toggweiler and Carson* [1995] the surface convergence takes place on either side of the equator and results in downwelling of the surface water. This hydrodynamical feature can explain the large extension in depth of the DON rich waters (>6.5 μg-at L^{-1} at 100 m, Figure 4f). At depth, DON may be remineralized as concluded from active ammonium regeneration (>100 ng-at L^{-1} d^{-1}) and ammonium accumulation found in this region (Figure 4h). Near-surface maxima of heterotrophic bacteria have been found centered around the convergence zone [*Landry et al.*, 1996] depicting this zone as an active region of remineralization. *Toggweiler and Carson*'s [1995] model suggests that downwelled water recirculates in the equatorial undercurrent at depths of 50–150 m back toward the equator. In our case, inorganic nitrogen resulting from DON remineralization could have been, in part, upwelled and thus have reached again the euphotic zone. This cell circulation between the equatorial upwelling, the poleward convergence, and the downwelling may efficiently maintain nitrogen in the system if the upwelling source is not deeper than 100–150 m. The only loss of organic matter from this system would be due to sinking particles which appear as a very low fraction of new production.

3.6.2. Does the equatorial cell circulation explain the HNLC situation? One of the remaining questions concerns why the phytoplankton biomass and productivity in the equatorial Pacific is not as high as the nitrate level could potentially support. Why is the equatorial Pacific not greener [*Barber*, 1992]? The small variations in chlorophyll compared to the large variations in the physical environment argue for a chemical and/or biological factor regulating chlorophyll concentration in the equatorial Pacific. While possible explanations, such as grazing [*Walsh*, 1976] and nutrient limitation by macronutrients or micronutrients, have been well discussed in literature, iron is actually the most likely candidate [*Lindley et al.*, 1995; *Martin et al.*, 1994; *Chavez and Smith*, 1995]. In our case the fact that the f ratio was lower than expected from nitrate

concentration might be explained by a greater effect of iron deficiency on nitrate uptake than on ammonium uptake. Several experiments of iron enrichment have recently demonstrated that only diatoms are stimulated by artificial iron addition [*Fitzwater et al.*, 1996; *Zettler et al.*, 1996]. From this observation, one may conclude that iron deficiency leads to the maintenance of a population trapped in a small-sized, low-sinking rate group of species that encourage grazing or the functioning of a microbial loop which in turn holds the residence time of the cells to about a day [*Cullen et al.*, 1992; *Wilkerson and Dugdale*, 1992]. *Peduzzi and Herndl* [1992] have shown that zooplankton grazing on phytoplankton fuels the microbial loop through the release of labile dissolved organic matter. The levels of ammonium regeneration measured in this study tend to confirm this hypothesis. At the equator, although ammonium concentrations were low (not high enough to inhibit nitrate uptake), ammonium regeneration (>150 ng-at L^{-1} d^{-1}) supplied enough nitrogen to sustain high phytoplanktonic growth rates. Considering a chlorophyll/nitrogen ratio of 1 for this region [*Eppley et al.*, 1992], the daily growth rate of regenerated ammonium was ~0.5–0.7 d^{-1}. However, we wish to point out the possible role played by new silicate in limiting primary productivity in the equatorial region, keeping in mind that "no single factor can be said to control phytoplankton to the exclusion to others" [*Chisholm and Morel*, 1991, Introduction]. We observed anomalies in the nitrogen/silicate ratio in surface waters between 0 and 5°S, suggesting a possible silicate limitation of diatom growth as noted in coastal upwelling [*Dugdale et al.*, 1995; *Copin-Montégut and Raimbault*, 1994] as well as in the equatorial Pacific divergence [*Dugdale and Wilkerson*, 1998]. Diatom biomass decreased to "background" levels at latitude 5°S [*Bidigare and Ondrusek*, 1996], and *Chavez* [1987] concluded that the occurrence of blooming is unlikely in the equatorial Pacific because of the absence of chain-forming diatoms. *Bender and McPhaden* [1990] have reported similar high nitrate/silicate ratios (>6.6) near the equator at 140°W in 1988 and suggested that this anomalous nutrient distribution resulted from rapid silicate removal by a transient biological event.

With the help of our chemical and biological data and recent data from literature we can propose a schematic picture of the functioning of the ecosystem of the central equatorial Pacific upwelling. Low utilization of available nitrate was likely the consequence of a grazing effect by microzooplankton as well as by mesozooplankton. Grazing would reduce the autotrophic biomass and absolute inorganic nitrogen consumption and also increase the availability of DON which could in turn stimulate the ammonium regeneration via heterotrophic bacteria [*Kirchman et al.*, 1989]. Since ammonium is generally the preferred form of nitrogen used by phytoplankton, especially by small-sized species, its availability may be an important regulator of new production in this nitrate rich environment. Thus the equatorial system is locked into a strong grazing loop dominated by small organisms <10μm [*Peña et al.*, 1991; *Chavez*, 1989], with virtually everyday's production consumed within the same period [*Cullen et al.*, 1992]. During some periods of intense upwelling, at times when the equatorial thermocline shoals and mixed layer nutrient concentration rises, diatom blooms might occur, leading to transient high new production associated with high silicate [*Bender and McPhaden*, 1990] and maybe iron consumption. While nitrogen is efficiently recycled via DON release and ammonium regeneration, a great part of silicate and maybe also of iron might leave the euphotic zone via sinking diatoms and might not be sufficiently remineralized. Evidence for rapid losses via vertical transport was apparent from deep sediment trap fluxes measured by *Honjo et al.* [1995] during the EqPac study in January 1992. Silicate-depleted waters could have entered into the "conveyor belt" meridional circulation. Consequently, when the perturbed system returns to equilibrium, surface waters at the equator, upwelled from low depths and in part fueled by surface water from the convergence, where nitrogen and maybe a great part of phosphorus and carbon are remineralized, have lost most of their silicate. This loss of particulate silicate and the recycling of only nitrogen via biological and physical processes may explain the deficiency in silicate observed in the upwelled water at the equator during El Niño events. Equatorial regions characterized by low silicate concentrations, i.e., NO_3/Si ratios $\gg 1$, and by high levels of ammonium and in situ nitrate regeneration can be qualified as a new Si-limited system [*Ku et al.*, 1995] where new production and export were mostly controlled by silicate. More data on nitrification, especially from the equatorial undercurrent, are required to fully elucidate the equatorial nitrogen cycle, while data on solid biogenic silica (opal) and iron in sediment particles are needed to understand better the origin of these macronutrient and micronutrient deficiencies. Therefore, in spite of significantly high new production at the equator compared to the oligotrophic system the net biological effect of the equatorial upwelling in the CO_2 export should be very weak but could be activated by a significant transient supply of silicate (and iron) forced by ocean circulation (strong shoaling of thermocline), thus initiating blooms of large sinking cells like diatoms.

Acknowledgments. The Oligotrophie en Pacifique (OLIPAC) cruise was a contribution to the JGOFS-France program in the equatorial Pacific and was included in the Etude des Processus dans l'Océan Pacifique Equatorial (EPOPE) program with the FLUx dans l'ouest du PACifique equatorial (FLUPAC) cruise (October 1994) mainly devoted to the study of the primary productivity along 165°E and along the equator between 165°E and 150°W. Funds came from the French organizations IFREMER, INSU, and by ORSTOM. We are grateful to the crew of the R/V *L'Atalante* for efficient help during the cruise. We wish to thank D. Taillez and C. Bournot for CTD data and for collecting samples of sediment traps and A. Morel and S. Maritorena for providing light data. We thank M. C. Bonin for drawing figures and contributing data from literature. The authors also thank the two anonymous referees, who helped to improve the final version of the manuscript.

References

Allen, C. B., J. Kanda, and E. A. Laws, New production and photosynthetic rates within and outside a cyclonic mesoscale eddy in the North Pacific subtropical gyre, *Deep Sea Res., Part II, 43*, 917–936, 1996.

Altabet, M. A., Organic C, N and stable isotopic composition of particulate matter collected on glass-fiber and aluminium oxide filters, *Limnol. Oceanogr., 35*, 902–909, 1990.

Antia, N. J., P. J. Harrison, and L. Oliveira, The role of dissolved organic matter in phytoplankton nutrition, cell biology and ecology, *Phycologia, 30*, 1–89, 1991.

Barber, R. T., Introduction to the WCE88 cruise: An investigation into why the equator is not greener, *J. Geophys. Res., 97*, 609–610, 1992.

Barber, R. T., M. P. Sanderson, S. T. Lindley, F. Chay, C. C. Trees, D. G. Foley, and F. P. Chavez, Primary productivity and its regulation in the equatorial Pacific during and following the 1991–1992, El Niño, *Deep Sea Res., Part II, 43*, 933–969, 1996.

Bender, M. L., and M. J. McPhaden, Anomalous nutrient distribution in the equatorial Pacific in April 80: Evidence for rapid biological uptake, *Deep Sea Res., Part A, 37*, 1075–1084, 1990.

Betzer, P. R., W. J. Showers, E. A. Laws, C. D. Wenn, G. R. Di Tullio, and P. M. Kroopnick, Primary productivity and particle fluxes on a transect of the equator at 153°W in the Pacific Ocean, *Deep Sea Res., Part A, 31*, 1–11, 1984.

Bidigare, R. R., and M. E. Ondrusek, Spatial and temporal variability of phytoplankton pigment distributions in the central equatorial Pacific Ocean, *Deep Sea Res., Part II, 43*, 809–833, 1996.

Bronk, D., and P. M. Glibert, Application of a ^{15}N tracer method to the study of dissolved organic nitrogen uptake during spring and summer in Chesapeake Bay, *Mar. Biol., 115*, 501–508, 1993.

Bronk, D. A., P. M. Glibert, and B. B. Ward, Nitrogen uptake, dissolved organic nitrogen release and new production, *Science, 265*, 1843–1846, 1994.

Buesseler, K. O., J. A. Andrews, M. C. Hartman, R. Belastock, and F. Chai, Regional estimates of the export flux of particulate organic carbon derived from thorium-243 during the JGOFS EqPac program, *Deep Sea Res., Part II, 42*, 777–804, 1995.

Carr, M.-E., N. S. Oakey, B. Jones, and M. R. Lewis, Hydrographic patterns and vertical mixing in the equatorial Pacific along 150°W, *J. Geophys. Res., 97*, 611–626, 1992.

Chavez, F. P., Size distribution of phytoplankton in the central and eastern tropical Pacific, *Global Biogeochem. Cycles, 3*, 27–35, 1989.

Chavez, F. P., and R. T. Barber, An estimate of new production in the equatorial Pacific, *Deep Sea Res., Part A, 34*, 1229–1243, 1987.

Chavez, F. P., and S. L. Smith, Biological and chemical consequences of open ocean upwelling, in *Upwelling in the Ocean: Modern Processes and Ancient Records*, edited by C. P. Summerhayes et al., pp. 149–170, John Wiley, New York, 1995.

Chavez, F. P., K. R. Buck, S. K. Service, J. Newton, and R. T. Barber, Phytoplankton variability in the central and eastern tropical Pacific, *Deep Sea Res., Part II, 43*, 835–970, 1996.

Chisholm, S. W., and F. M. M. Morel, What controls phytoplankton production in nutrient-rich areas of the open ocean?, *Limnol. Oceanogr., 36*, 1507–1970, 1991.

Copin-Montégut, G., and B. Avril, Vertical distribution and temporal variation of dissolved organic carbon in the north-western Mediterranean Sea, *Deep Sea Res., Part I, 40*, 1963–1972, 1993.

Copin-Montégut, C., and P. Raimbault, The Peruvian upwelling near 15°S in August 1986: Results of continuous measurements of physical and chemical properties between 0 and 200 m depth, *Deep Sea Res., Part I, 41*, 439–467, 1994.

Cullen, J. J., M. R. Lewis, C. O. Davis, and R. T. Barber, Photosynthetic characteristics and estimated growth rates indicate grazing is the proximate control of primary production in the equatorial Pacific, *J. Geophys. Res., 97*, 639–654, 1992.

Deuser, W. G., E. H. Ross, and R. F. Anderson, Seasonality in the supply of sediment to the deep Sargasso Sea, and implications for the rapid transfer of matter to the deep ocean, *Deep Sea Res., Part A, 28*, 495–505, 1981.

Dugdale, R. C., and J. J. Goering, Uptake of new and regenerated forms of nitrogen in primary productivity, *Limnol. Oceanogr., 12*, 196–206, 1967.

Dugdale, R. C., and F. P. Wilkerson, The use of ^{15}N to measure nitrogen uptake in eutrophic oceans, experimental considerations, *Limnol. Oceanogr., 31*, 673–689, 1986.

Dugdale, R. C., and F. P. Wilkerson, Silicate regulation of new production in the equatorial Pacific upwelling, *Nature, 311*, 270–273, 1998.

Dugdale, R. C., F. P. Wilkerson, F. P. Chavez, and R. T. Barber, Estimating new production in the equatorial Pacific at 150°W, *J. Geophys. Res., 97*, 681–686, 1992.

Dugdale, R. C., F. P. Wilkerson, and H. J. Minas, The role of a silicate pump in diving new production, *Deep Sea Res., Part I, 42*, 697–719, 1995.

Eppley, R. W., and B. J. Peterson, Particulate organic matter flux and planktonic new production in the deep ocean, *Nature, 282*, 677–680, 1979.

Eppley, R. W., F. P. Chavez, and T. R. Barber, Standing stocks of particulate carbon and nitrogen in the equatorial Pacific at 150°W, *J. Geophys. Res., 97*, 655–661, 1992.

Fitzwater, S. E., K. H. Coale, R. M. Gordon, K. S. Johnson, and M. E. Ondrusek, Iron deficiency and phytoplankton growth in the equatorial Pacific, *Deep Sea Res., Part II, 43*, 995–1015, 1996.

Fleming, R. H., The composition of plankton and units for reporting population and production, paper presented at Sixth Pacific Science Congress, Sears Foundation, San Francisco, Calif., 1939.

Gentilhomme, V., and P. Raimbault, Absorption et régénération de l'azote dans la zone frontale du courant algérien (Méditerranée ocidentale): Réévaluation de la production nouvelle, *Oceanol. Acta, 17*, 555–562, 1994.

Glibert, P. M., F. Lipschultz, J. J. McCarthy, and M. A. Altabet, Isotope dilution models of uptake and remineralization of ammonium by marine plankton, *Limnol. Oceanogr., 27*, 639–650, 1982.

Harrison, W. G., L. R. Harris, and B. D. Irwin, The kinetics of nitrogen utilization in the oceanic mixed layer: Nitrate and ammonium interactions at nanomolar concentrations, *Limnol. Oceanogr., 41*, 16–32, 1996.

Honjo, S., J. Dymond, R. Collier, and S. J. Manganini, Export production of particles to the interior of the equatorial Pacific Ocean during the 1992 EqPac experiment, *Deep Sea Res., Part II, 42*, 831–870, 1995.

Kessler, W. S., and M. J. McPhaden, The 1991–1993 El Niño in the central Pacific, *Deep Sea Res., Part II, 42*, 295–333, 1995.

Kirchman, D. L., R. G. Keil, and P. A. Wheeler, The effect of amino acids on ammonium utilization and regeneration by heterotrophic bacteria in the subarctic Pacific, *Deep Sea Res., Part A, 36*, 1763–1776, 1989.

Knauer, G. A., J. H. Martin, and K. W. Bruland, Fluxes of particulate carbon, nitrogen and phosphorus in the upper water column of the northeast Pacific, *Deep Sea Res., Part A, 37*, 1121–1134, 1979.

Ku, T. L., S. Luo, M. Kusakabe, and J. K. B. Bishop, ^{228}Ra derived nutrient budgets in the upper equatorial Pacific and the role of "new" silicate in limiting productivity, *Deep Sea Res., Part II, 42*, 479–498, 1995.

Landry, M. R., J. D. Kirshtein, and J. Constantinou, Abundances and distributions of picoplankton populations in the central equatorial Pacific from 12°N to 12°S, 140°W, *Deep Sea Res., Part II, 43*, 871–890, 1996.

Libby, P. S., and P. A. Wheeler, Particulate and dissolved organic nitrogen in the central and eastern equatorial Pacific, *Deep Sea Res., Part I, 44*, 345–361, 1997.

Lindley, S. T., R. R. Bidigare, and R. T. Barber, Phytoplankton photosynthesis parameters along 140°W in the equatorial Pacific, *Deep Sea Res., Part II, 42*, 441–464, 1995.

Lohrenz, S. E., G. A. Knauer, V. L. Asper, M. Tuel, A. F. Michaels, and A. H. Knap, Seasonal variability in primary production and particle flux in the northwestern Sargasso Sea: US JGOFS Bermuda Atlantic Time-Series Study, *Deep Sea Res., Part A, 39*, 1373–1391, 1992.

Luo, S., T. L. Ku, M. Kusakabe, J. K. B. Bishop, and Y. L. Yang, Tracing particle cycling in the upper ocean with ^{230}Th and ^{228}Th: An investigation in the equatorial Pacific along 140°W, *Deep Sea Res., Part II, 42*, 805–830, 1995.

Martin, J. H., Glacial-interglacial CO_2 change: The iron hypothesis, *Paleooceanography, 5*, 1–13, 1990.

Martin, J. H., et al., Testing the iron hypothesis in ecosystems of the equatorial Pacific Ocean, *Nature, 371*, 123–129, 1994.

McCarthy, J. J., C. Garside, J. L. Nevins, and R. T. Barber, New production along 140°W in the equatorial Pacific during and after the 1992 El Niño event, *Deep Sea Res., Part II, 43*, 1065–1093, 1996.

Minas, H. J., M. Minas, and T. T. Packard, Productivity in upwelling areas deduced from hydrographic and chemical fields, *Limnol. Oceanogr., 31*, 1182–1206, 1986.

Murray, J. W., J. Downs, S. Strom, C. L. Wei, and H. Jannasch, Nutrient assimilation, export production and ^{234}Th scavenging in the eastern equatorial Pacific, *Deep Sea Res., Part A, 36*, 1471–1489, 1989.

Murray, J. W., R. T. Barber, M. R. Roman, M. P. Bacon, and R. A. Feely, Physical and biological controls on carbon cycling in the equatorial Pacific, *Science, 266*, 58–65, 1994.

Murray, J. W., E. Johnson, and C. Garside, A U.S. JGOFS process study in the equatorial Pacific (EqPac): Introduction, *Deep Sea Res., Part II, 42*, 275–293, 1995.

Murray, J. W., J. Young, J. Newton, J. Dunne, T. Chapin, B. Paul, and J. J. McCarthy, Export flux of particulate organic carbon from the central equatorial Pacific determined using a combined drifting trap-^{234}Th approach, *Deep Sea Res., Part II, 43*, 1095–1132, 1996.

Peduzzi, P., and G. J. Herndl, Zooplankton activity fueling the microbial loop-differential growth response of bacteria from oligotrophic and eutrophic waters, *Limnol. Oceanogr., 37*, 1087–1092, 1992.

Peltzer, E. T., and N. A. Hayward, Spatial and temporal variability of

total organic carbon along 140°W in the equatorial Pacific Ocean in 1992, *Deep Sea Res., 43, Part II, 43*, 1155–1180, 1996.

Peña, M. A., M. R. Lewis, and W. G. Harrison, Particulate organic matter and chlorophyll in the surface layer of the equatorial Pacific Ocean along 135°W, *Mar. Ecol. Prog. Ser., 72*, 179–188, 1991.

Peña, M. A., M. R. Lewis, and W. G. Harrison, Primary productivity and size structure of phytoplankton biomass on a transect of the equator at 135°W in the Pacific Ocean, *Deep Sea Res., Part A, 37*, 295–315, 1992a.

Peña, M. A., W. G. Harrison, and M. R. Lewis, New production in the central equatorial Pacific, *Mar. Ecol. Prog. Ser., 80*, 265–274, 1992b.

Platt, T. T., and W. G. Harrison, Biogenic fluxes of carbon and nitrogen in the ocean, *Nature, 318*, 55–58, 1985.

Preston, T., and N. J. P. Owens, Interfacing an elemental analyzer with an isotope ratio mass spectrometer: The potential for fully automated total nitrogen and nitrogen-15 analysis, *Analyst, 108*, 971–977, 1983.

Pujo-Pay, M., and P. Raimbault, Improvement of the wet-oxidation procedure for the simultaneous determination of particulate organic nitrogen and phosphorus collected on filters, *Mar. Ecol. Prog. Ser., 105*, 203–207, 1994.

Pujo-Pay, M., P. Raimbault, and P. Conan, Underestimation of particulate nitrogen concentrations in the open ocean by the use of GF/F filters, *C.R. Acad Sci., Sec. II, 324*, 401–407, 1997.

Raimbault, P., I. Taupier-Letage, and M. Rodier, Vertical size distribution of phytoplankton in the western Mediterranean Sea during early summer, *Mar. Ecol. Prog. Ser., 45*, 153–158, 1988.

Raimbault P., G. Slawyk, B. Coste, and J. Fry, Feasibility of using an automated procedure for the determination of seawater nitrate in the 0–100 nM range: Examples from field and cultures, *Mar. Biol., 104*, 347–351, 1990.

Slawyk, G., and P. Raimbault, A simple procedure for simultaneous recovery of dissolved inorganic and organic nitrogen in ^{15}N-tracer experiments and improving the isotopic mass balance, *Mar. Ecol. Prog. Ser., 124*, 289–299, 1995.

Slawyk, G., P. Raimbault, and N. Garcia, Measuring gross uptake of ^{15}N-labeled nitrogen by marine phytoplankton without particulate matter collection: Evidence of low ^{15}N losses to the dissolved organic nitrogen pool, *Limnol. Oceanogr.*, in press, 1999.

Suess, E., Particulate organic carbon flux in the oceans: Surface productivity and oxygen utilization, *Nature, 288*, 260–263, 1980.

Tans, P., I. Y. Fung, and T. Takahashi, Observational constraints on the global atmospheric CO_2 budget, *Science, 247*, 1431–1438, 1990.

Thomas, W. H., Nutrient inversions in the southeastern tropical Pacific Ocean, *Fish. Bull., 70*, 929–932, 1972.

Thomas, W. H., Anomalous nutrient-chlorophyll interrelationships in the offshore eastern tropical Pacific Ocean, *J. Mar. Res., 37*, 327–335, 1979.

Toggweiler, J. R., Is the downward dissolved organic matter (DOM) flux important in carbon export, in *Productivity of the Ocean: Present and Past*, edited by W. H. Berger et al., pp. 65–84, Wiley-Intersci., New York, 1989.

Toggweiler, J. R., and S. Carson, What are upwelling systems contributing to the ocean's carbon and nutrient budgets? in *Upwelling in the Ocean: Modern Processes and Ancient Records*, edited by C. P. Summerhayes et al., pp. 337–360, John Wiley, New York, 1995.

Tréguer, P., and P. LeCorre, *Manuel d'Analyse Des Sels Nutritifs Dans l'Eau de Mer: Utilisation de l'AutoAnalyser II Technicon*, 2nd ed., Univ. of Bretagne Occidentale, Lab. de Chim. Mar., Brest, France, 1975.

Wafar, M. V. M., P. Le Corre, and S. L'Helguen, *f*-ratios calculated with and without urea uptake in nitrogen uptake by phytoplankton, *Deep Sea Res.*, Part I, *42*, 1669–1674, 1995.

Walsh, J. J., Herbivory as a factor in patterns of nutrient utilization in the sea, *Limnol. Oceanogr., 21*, 1–13, 1976.

Ward, B. B., Light and substrate concentration relationship with marine assimilation and oxidation rates, *Mar. Chem., 16*, 301–316, 1985.

Wilkerson, F. P., and R. C. Dugdale, Measurements of nitrogen productivity in the equatorial Pacific, *J. Geophys. Res., 97*, 669–680, 1992.

Wyrtki, K., and B. Kilonsky, Mean water and current structure during the Hawaii-to-Tahiti shuttle experiment, *J. Phys. Oceanogr., 14*, 242–254, 1984.

Zettler, E. R., R. J. Olson, B. J. Binder, S. W. Chisholm, S. E. Fitzwater, and R. M. Gordon, Iron-enrichment bottle experiments in the equatorial Pacific: Responses of individual phytoplankton cells, *Deep Sea Res., Part II, 43*, 1017–1029, 1996.

B. Boudjellal, Institut des Sciences de la Mer et de l'Aménagement du Littoral, B.P. 54, Sidi Fredj, Staouel: 42321, Algérie.

C. Coatanoan, P. Conan, B. Coste, N. Garcia, T. Moutin, M. Pujo-Pay, P. Raimbault, and G. Slawyk, Laboratoire d'Océanographie et de Biogéochimie (UMR CNRS 6535), Centre d'Océanologie de Marseille, Campus de Luminy, F-13288 Marseille Cedex, France. (raimbault@com.univ-mrs.fr)

(Received September 8, 1997; revised August 10, 1998; accepted August 31, 1998.)